AGU PUBLICATIONS

JGR

Journal of Geophysical Research: Atmospheres

RESEARCH ARTICLE
10.1002/2014JD023033

Key Points:
- Aerosol-thermodynamic-convective cloud interactions are investigated
- Higher CCN concentrations and greater NCAPE lead to stronger convection
- Warm cloud depth modulates NCAPE-CCN-convection interplay

Correspondence to:
D. C. Stolz,
dstolz@atmos.colostate.edu

Citation:
Stolz, D. C., S. A. Rutledge, and J. R. Pierce (2015), Simultaneous influences of thermodynamics and aerosols on deep convection and lightning in the tropics, *J. Geophys. Res. Atmos.*, *120*, 6207–6231, doi:10.1002/2014JD023033.

Received 30 DEC 2014
Accepted 29 MAY 2015
Accepted article online 3 JUN 2015
Published online 29 JUN 2015

©2015. American Geophysical Union. All Rights Reserved.

Simultaneous influences of thermodynamics and aerosols on deep convection and lightning in the tropics

Douglas C. Stolz[1], Steven A. Rutledge[1], and Jeffrey R. Pierce[1]

[1]Department of Atmospheric Science, Colorado State University, Fort Collins, Colorado, USA

Abstract Convective features (CFs) observed by the Tropical Rainfall Measuring Mission satellite between 2004 and 2011 are analyzed to determine the relative roles of thermodynamics and aerosols as they modulate radar reflectivity and lightning. We studied the simultaneous impacts of normalized convective available potential energy (NCAPE) and warm cloud depth (WCD) as well as cloud condensation nuclei concentrations ($D \geq 40$ nm; N40) on total lightning density (TLD), average height of 30 dBZ echoes (AVGHT30), and vertical profiles of radar reflectivity (VPRR) within individual CFs. The results show that TLD increases by up to 600% and AVGHT30 increases by up to 2–3 km with increasing NCAPE and N40 for fixed WCD. The partial sensitivities of TLD/AVGHT30 to NCAPE and N40 separately were comparable in magnitude but account for a fraction of the total range of variability (i.e., when the influences of NCAPE and N40 are considered simultaneously). Both TLD and AVGHT30 vary inversely with WCD such that maxima of TLD and AVGHT30 are found for *the combination of high NCAPE, high N40, and shallower WCD*. The relationship between lightning and radar reflectivity was shown to vary as a function of N40 for a fixed thermodynamic environment. Analysis of VPRRs shows that reflectivity in the mixed phase region is up to 5.0–5.6 dB greater for CFs in polluted environments compared to CFs in pristine environments (holding thermodynamics fixed). This analysis favors a merged hypothesis for the simultaneous roles of thermodynamics and aerosols as they influence deep convective clouds in the Tropics.

1. Introduction

Over the past several decades, satellite observations have proven to be indispensable for characterizing convective clouds in the Tropics and subtropics. Climatologies derived from the burgeoning data record have identified several important findings surrounding the phenomenon of deep convection. One prominent result is that lightning-producing convective features (LPCFs) occur predominantly over continental regions in the Tropics, whereas the majority of precipitating features occur over tropical ocean [*Orville and Henderson*, 1986; *Mackerras et al.*, 1998; *Boccippio et al.*, 2000, 2005; *Christian et al.*, 2003; *Cecil et al.*, 2005]. *Boccippio et al.* [2000] refined the understanding when they conducted an individual convective feature-based analysis across the Tropics and concluded that total lightning rates in continental thunderstorms are a factor of 2–3 larger compared to oceanic thunderstorms.

Regional analyses employing satellite instruments and ground-based radars have documented distinct differences in vertical precipitation structure throughout the Tropics associated primarily with intraseasonal variability [*Szoke et al.*, 1986; *Williams et al.*, 1992; *Rutledge et al.*, 1992; *Zipser and Lutz*, 1994; *Petersen et al.*, 1996; *DeMott and Rutledge*, 1998; *Rosenfeld and Lensky*, 1998; *Petersen and Rutledge*, 2001; *Cifelli et al.*, 2002; *Williams et al.*, 2002; *Petersen et al.*, 2006]. *Petersen and Rutledge* [2001] found a continuum of vertical reflectivity distributions corresponding to remote oceanic, coastal, and continental convection. A key finding was the higher frequency-of-occurrence of 30 dBZ radar echoes at temperatures colder than −10°C (greater than ~6 km mean sea level) in tropical continental convection (compared to tropical oceanic convection). The relative frequency of 30 dBZ echoes at these heights was considerably less over coastal and (especially) over remote oceanic regions.

In turn, these disparities in vertical precipitation structure have been related to appreciable differences in lightning. On average, deep convection that produces significant amounts of lightning is frequently the most vertically developed from the radar perspective [*Dye et al.*, 1989; *Rutledge et al.*, 1992; *Williams et al.*, 1992; *Zipser*, 1994; *Petersen et al.*, 1996; *Carey and Rutledge*, 2000; *Nesbitt et al.*, 2000; *Cecil et al.*, 2005; *Zipser et al.*, 2006; *Liu et al.*, 2012; *Stolz et al.*, 2014], whereas reduced lightning activity in deep convection is

often associated with reduced reflectivities above the freezing level. Such close correspondence between lightning and radar characteristics is substantiated by both theoretical and laboratory studies which support the noninductive mechanism (charge separation that occurs during collisions between ice particles in the presence of supercooled liquid within a cloud's mixed phase region). It is generally accepted that this mechanism is the most plausible explanation for lightning initiation [*Reynolds et al*., 1957; *Takahashi*, 1978; *Baker et al*., 1987; *Saunders*, 1993; *Baker and Dash*, 1994]. Indeed, global distributions of ice-water path observed using satellites exhibit strong correlations with lightning and radar echo top climatology [*Petersen and Rutledge*, 2001; *Petersen et al*., 2005].

Thus, a multitude of observations clearly illustrate fundamental differences in the makeup and electrical behavior of deep convection between tropical continental and oceanic regions. We are then left to question the underlying driver(s) of the observed variability in lightning and convective intensity. There are two hypotheses in the literature—the thermal hypothesis and the aerosol hypothesis—that attempt to explain the aforementioned variability.

The thermal hypothesis holds that the variability in lightning and convective intensity over continental and oceanic regions in the Tropics can be explained by differences in thermodynamic instability [*Rutledge et al*., 1992; *Williams et al*., 1992, 2002; *Williams and Stanfill*, 2002; *Williams and Sátori*, 2004]. One major caveat to the thermal hypothesis has been demonstrated in a number of analyses: the average convective available potential energy (CAPE), which represents the column-integrated energy available to accelerate parcels vertically, *is approximately the same over continents and oceans* [*Williams and Renno*, 1993; *Lucas et al*., 1994a, 1994b; *Halverson et al*., 2002; *Williams and Stanfill*, 2002]. *Williams and Stanfill* [2002] argue that tropical land surfaces, with their relatively low heat capacity and high Bowen ratio, respond strongly to solar radiation and excite larger, more buoyant (energetic) parcels which ascend through a deep boundary layer and therefore are less susceptible to dilution via entrainment. Parcels in oceanic regimes have reduced thermal buoyancy in the lower and middle troposphere and may undergo more significant entrainment as a direct consequence of smaller parcel widths, resulting from ascent through a shallower boundary layer. The differences would suggest that mixed phase microphysics and noninductive charging are both more robust in continental convection compared to oceanic convection, as wider updrafts contribute to a more efficient conversion of CAPE to updraft kinetic energy [e.g., *Williams et al*., 2005]. *Williams et al*. [2005] found that flash rates increased with increasing cloud base height for a sample of tropical convective clouds (i.e., assuming that updraft width is proportional to cloud base height).

Advocates of the aerosol hypothesis argue that the number of cloud condensation nuclei (CCN) in the environment of convective clouds significantly influences their microphysical and vertical development [*Rosenfeld and Lensky*, 1998; *Rosenfeld*, 1999; *Ramanathan*, 2001; *Andreae et al*., 2004; *Graf*, 2004; *Lohmann and Feichter*, 2005; *Sherwood et al*., 2006; *Hudson and Mishra*, 2007; *Andreae and Rosenfeld*, 2008; *Bell et al*., 2008; *Lee et al*., 2008; *Rosenfeld et al*., 2008, hereafter R08; *Koren et al*., 2010, 2012; *Li et al*., 2011; *May et al*., 2011; *Yuan et al*., 2011, 2012; *Heiblum et al*., 2012; *Niu and Li*, 2012; *Fan et al*., 2013; *Lebo and Morrison*, 2014; *Storer et al*., 2014; *Wall et al*., 2014]. In their theoretical work, R08 provided a conceptual description of so-called aerosol-induced convective invigoration which has since been cited in many studies on the subject. Following their model, in convective clouds that develop in an environment with high aerosol concentrations ($>500\,\mathrm{CCN\,cm^{-3}}$), precipitation formation by the collision-coalescence mechanism is hindered relative to clouds drawing on lower CCN concentrations. Substantial cloud water is then transported above the freezing level which upon freezing releases latent heat contributing to increased thermal buoyancy, stronger vertical motions, and greater charge separation. Note that R08 also emphasize the importance of offloading condensate in order for the maximum invigoration effect to be realized in and above the mixed phase region (see Figure 3 of that study). In more pristine environments ($<100\,\mathrm{CCN\,cm^{-3}}$), collision/coalescence becomes very efficient which leads to rapid generation of precipitation, thereby reducing supercooled water contents in the mixed phase region. This may explain the relatively low occurrence of lightning over remote oceanic regions.

We hypothesize that warm cloud depth (WCD), defined as the vertical distance between the lifted-condensation level (LCL) and the freezing level, could simultaneously influence the growth of cloud droplets by determining the duration of ascent through a cloud's warm phase and the subsequent development of precipitation by condensation or collision/coalescence [e.g., *Carey and Buffalo*, 2007] in combination with

aerosol indirect effects. *Takahashi* [1978] communicated the importance of liquid water content for the charge separation process. For deep WCD, a relatively long trajectory through the cloud's warm phase implies that the probability of precipitation formation increases as autoconversion proceeds; therefore, cloud liquid may be lost prior to its arrival in the mixed phase region where charge separation may decrease subsequently. Conversely, for shallower WCD, the likelihood that more cloud liquid reaches the mixed phase increases for a fixed updraft and aerosol concentration. Lastly, for very shallow WCD (most applicable outside the Tropics), the duration of ascent through a cloud's warm phase is shortest for a fixed updraft velocity. In this case, the time period during which aerosols may be able to impact collision/coalescence is short, and as a result, there may be little if any sensitivity to aerosol concentration [e.g., *Li et al*., 2011].

These ideas are supported by a number of model-based analyses of the impacts of aerosols on convective clouds in environments where WCD ranges from shallow to deep. *Fan et al*. [2007] found that the influence of aerosols on the microphysical development of deep convective clouds was negligible when surface dew-point temperature depressions were large (i.e., dry boundary layers with resulting shallower WCD). In 3-D simulations of convective clouds in the deep Tropics (where WCD is deep), *Wang* [2005] found increasing precipitation as the initial CCN concentration was varied from 50 cm^{-3} to more than 5000 cm^{-3}, but decreases in precipitation efficiency were not observed even under heavily polluted conditions. In contrast, 2-D simulations of isolated convection in environments with intermediate WCD (WCD ~2 km) depicted increases in max updraft velocity of 5–6 $m\,s^{-1}$ and enhanced lightning as aerosol concentrations were increased from 50 to $>$500 cm^{-3} [*Mansell and Ziegler*, 2013].

Results from regional and cloud-resolving model studies that investigate the robustness of aerosol effects in varied thermodynamic environments throughout the Tropics and subtropics depict nontrivial modifications to a cloud's hydrometeor population and subsequent dynamics [*Khain et al*., 2005, 2012; *van den Heever et al*., 2006; *van den Heever and Cotton*, 2007; *Lee et al*., 2008; *Fan et al*., 2013; *Storer and van den Heever*, 2013; *Venevsky*, 2014]. These results generally show enhanced pristine ice, as well as increases in graupel and hail at the expense of rain and drizzle in the cloud's warm phase when aerosol concentrations exceed ~100–400 cm^{-3} [e.g., *Storer and van den Heever*, 2013]. Collectively, these studies strengthen the case for aerosol effects on deep convection and lightning, but considerable uncertainty remains [e.g., *Stevens and Feingold*, 2009; *van den Heever et al*., 2011; *Lee*, 2012; *Wall et al*., 2014]. For example, differences in precipitation/updraft intensity within an individual cloud with respect to changes in aerosol concentrations may be buffered [e.g., *Stevens and Feingold*, 2009] or overwhelmed by the compensating circulations in the ensemble of deep convective clouds across a wider domain [e.g., *Lee*, 2012].

In their recent global analysis of the impacts of aerosol indirect effects on convective clouds, *Wall et al*. [2014] concluded, "…the true magnitude of the aerosol indirect effect [on deep convection] remains elusive on the global scale." They demonstrated regional sensitivity of deep convective clouds to aerosol load in the atmospheric column while accounting for meteorological factors, but their uncertainty may be the result of their choice to use column-integrated aerosol quantities estimated from satellites. Wall et al. were diligent in addressing the limitations of their chosen satellite aerosol data [e.g., *Várnai et al*., 2013], but other investigators have found aerosol number concentrations to be more illustrative in studies of aerosol-convection interactions [e.g., *Hudson and Mishra*, 2007; *Koren et al*., 2010].

We recognize that there may be a mutual dependence between aerosols and thermodynamics that leads to stronger convection. Following R08, aerosols may influence how much of the thermodynamic potential energy (i.e., CAPE) is realized by a parcel within a mature deep convective cloud. They argue that a shift from invigorated to suppressed convection should occur as a function of aerosol concentrations (as was exemplified by *Altaratz et al*. [2010], over the Amazon). According to R08, the optimum aerosol load is that which balances the effects of modifying hydrometeor size distributions and subsequent differences in latent heating against water loading within rising parcels. From another point of view, the environmental thermodynamics dictate whether aerosol indirect effects on deep convection will be significant [e.g., *Morrison and Grabowski*, 2013]. In the absence of large-scale forcing (i.e., within baroclinic zones or due to topography), conditional instability in the thermodynamic environment is necessary to accelerate parcels with variable aerosol concentrations to their respective LCLs and potentially to subfreezing temperatures in order for any microphysical response to aerosols to be observed.

This study addresses the question of how aerosols impact characteristics of deep convective clouds and attendant lightning production in the Tropics (over continents and oceans). Based on the above reasoning, we will consider the impacts of aerosols within the context of thermodynamic instability and WCD. Hence, we investigate the hypothesis that aerosols modulate the amount of available potential energy realized throughout the life cycle of a convective cloud and this interaction is sensitive to WCD. We utilize reanalysis and the GEOS-Chem transport model to estimate relevant thermodynamic and boundary layer aerosol number concentrations globally in lieu of satellite methods for retrieving environmental thermodynamic and aerosol characteristics. By this method, we assure a large, representative sample of deep convective clouds in the Tropics. Additionally, we contribute new insight about the simultaneous importance of WCD. Section 2 describes the multiple sources of data chosen for this investigation. Section 3 presents our examination of the sensitivity of lightning and radar characteristics of deep convective clouds to simultaneous estimates of normalized CAPE, boundary layer CCN, and WCD. Sections 4 and 5 provide a discussion of the results and conclusions, respectively.

2. Data and Methodology

We employ data from the Tropical Rainfall Measuring Mission (TRMM), which in itself represents the most spatially and temporally comprehensive, global-scale data set consisting of simultaneous high-resolution lightning and radar observations [TRMM precipitation radar (PR) and lightning imaging sensor (LIS) observations span all longitudes between 36°N-36°S and 38°N-38°S, respectively]. The TRMM Convective Feature (CF) database (available at http://trmm.chpc.utah.edu) is composed of individual groups of contiguous convective pixels observed by the TRMM PR that are determined by version 7 of the 2A23 "raintype" PR algorithm. A number of relevant radar and lightning characteristics are defined for each CF (e.g., maximum height of reflectivity echo tops, total lightning flash count, estimated time within the satellite's field of view, and number of PR pixels within the CF). The TRMM LIS detects total lightning, i.e., contributions from intracloud and cloud-to-ground lightning sources, but is unable to distinguish between the two types of lightning. An 8-year temporal subset (2004–2011) of the full CF database (1998–2014) was chosen to maximize overlap with the available global GFED3 biomass burning inventory [*van der Werf et al*., 2010] for the development of the aerosol data component, which will be described next.

A novel aspect of this research is its reliance on a global chemical transport model, GEOS-Chem (www.geos-chem.org) with the online aerosol microphysics module TOMAS [*Adams and Seinfeld*, 2002; *Pierce and Adams*, 2009; *D'Andrea et al*., 2013; *Pierce et al*., 2013], to provide estimates of lower tropospheric aerosol number concentrations on the global scale. GEOS-Chem-TOMAS simulates the particle size distribution from 3 nm to 10 μm in 15 size bins, and it tracks sulfate, sea salt, organics, black carbon, and dust aerosol species within these size sections. In this analysis, we use the GEOS-Chem-TOMAS aerosol fields to provide the simulated number concentration of aerosols with diameters larger than 40 nm ($D \geq 0.04$ μm). We refer to this concentration as N40. Thus, in this study, we do not account for differences in aerosol composition because the integrated number above cutoff diameters (as well as variability in maximum supersaturations) accounts for most of the variability in cloud droplet number concentrations [*Dusek et al*., 2006]. We expect that variability with respect to different aerosol species (e.g., giant CCN from sea spray, black carbon, and dust) could affect our results, and these sensitivities should be explored in future work.

In an analysis of particulate matter present within a variety of continental and marine air masses, *Dusek et al*. [2006] found that the CCN efficiency (i.e., the ratio of CCN to cloud nuclei) of aerosols with diameters larger than 40 nm was strongly sensitive to the level of supersaturation within cloudy parcels. For low supersaturations (<1%), N40 was shown to overestimate CCN concentrations, while for supersaturations a few tenths of a percent higher than 1%, the CCN efficiency of N40 rapidly increased up to values exceeding 0.8. Both observations and two-dimensional cloud scale simulations of growing congestus and cumulonimbus clouds in the Tropics show that supersaturations at various heights above cloud base range from a few tenths of a percent up to 3% or more [*Khain et al*., 2012, 2013]. This study focuses on deep convective clouds with strong updrafts that are capable of producing high supersaturations immediately above cloud base. Therefore, N40 should be an appropriate proxy for CCN in the context of this investigation; note that several aspects of this analysis were also conducted using N80 data from the GEOS-Chem model runs and the results were approximately unchanged (the correlation between N40 and N80 in our data sample was high, $r > 0.93$).

The simulations were run globally at a horizontal resolution of 2.5 degrees longitude by 2 degrees latitude (roughly 270 km by 220 km at the equator) for 47 vertical levels between approximately 1000 and 0.01 hPa. In our analysis, we use output between the 1000 and 850 hPa levels (10 layers). Output was provided every 6 h during the time period of interest over the domain spanning all longitudes and between the latitudes 38°S and 38°N (corresponding to the latitudinal extent of coverage for the TRMM LIS instrument). The spatial and temporal autocorrelation of aerosol quantities has been shown to be near 0.8 for time and space scales of 200 km and 10 h, respectively, in global observations [*Anderson et al.*, 2003]. Therefore, the model resolution should adequately capture aerosol variability on the scales of interest for the current study.

Our choice to use a chemical transport model arose from the documented uncertainties surrounding global satellite aerosol retrievals. We require observations as close as possible to deep convective clouds, but the probability of contamination for passive retrievals of aerosol characteristics by a satellite increases with decreasing distance to clouds [e.g., *Koren et al.*, 2010]. Additionally, passive imagers flying onboard satellites suffer from the inability to discern where in the atmospheric column the radiation reflected by aerosols originates and have difficulty differentiating aerosols from clouds, especially over land surfaces and near optically thick clouds where 3-D radiative effects are significant [*Varnai and Marshak*, 2009; *Várnai et al.*, 2013].

Errors in GEOS-Chem-simulated aerosol fields may impact the aerosol-cloud relationships determined in this analysis. If errors in aerosol variability are independent of cloud/lightning variability (e.g., random noise in the predicted aerosol fields as opposed to systematic bias), then the errors will contribute to reduced sensitivity in the trends of convective cloud characteristics versus aerosol concentrations. Therefore, we argue that our results should represent a lower bound for quantifying the influence of aerosols on the microphysical development of deep convective clouds and lightning production. In an independent assessment of the performance of the GEOS-Chem model [e.g., *D'Andrea et al.*, 2013], a comparison of predicted and observed aerosol concentrations at 21 ground sites throughout North America and Europe illustrated that the log-mean bias of predicted N40 in GEOS-Chem was less than ~|0.067| (a factor of ~1.17) for all sensitivity experiments conducted.

The CF database incorporates thermodynamic information from the Interim Reanalysis (ERAi) developed by the European Center for Medium Range Weather Forecasts (ECMWF) [*Dee et al.*, 2011]. For each CF, 10 levels of meteorological variables (1000–100 hPa) (Independent sensitivity analysis illustrated that the global probability distribution of CAPE computed using all 37 levels of available reanalysis data is more accurately reproduced using just 16 levels of thermodynamic data (1000, 975, 950, 925, 900, 850, 800, 750, 700, 600, 500, 400, 300, 250, 200, and 100 hPa) as opposed to the original 10 levels. In the interest of computational efficiency, the aforementioned 16 levels of data were chosen at 2.5° horizontal resolution for this analysis.) are provided from the nearest neighboring reanalysis grid point. These variables are linearly interpolated to the time of the TRMM overpass and are used to compute thermodynamic variables of interest. Global aerosol climatology and satellite observations of aerosols have been integrated into the ECMWF's data assimilation plan [*Morcrette et al.*, 2009; *Benedetti et al.*, 2009] and are accounted for in the radiative transfer scheme within the model [*Dee et al.*, 2011].

The methods for computing aerosol and thermodynamic quantities and attributing them to individual CFs will now be described in more detail. For each CF between the years 2004 and 2011 (inclusive), we computed a vector average of the horizontal wind components from ERAi reanalysis between 1000 and 850 hPa. We then defined an arbitrary "inflow" swath by a 90° sector centered on the computed direction (0–360°, with a direction of 360° denoting north). Next, the direction to all aerosol grid points relative to the geographic coordinates of each CF was calculated, and the grid points within the upstream swath sector at a distance of less than 350 km were identified. After linearly interpolating the aerosol data to the time of the TRMM overpass, boundary layer average (~1000–850 hPa) CCN concentrations (N40) were computed at the identified grid points and averaged. The average of boundary layer N40 in the upstream swath was then assigned to individual CFs.

ERAi profiles of temperature and moisture at the nearest reanalysis grid point within the upstream swath were used to calculate mixed-layer (lowest 50 hPa) pseudoadiabatic CAPE. The differences between the geopotential heights of the approximate levels of free convection and neutral buoyancy within each reanalysis sounding were found; this quantity represents the depth over which the idealized parcel's

perturbation temperature was positive. Normalized CAPE (NCAPE) was determined for each CF by dividing the mixed-layer pseudoadiabatic CAPE by the depth of the positive area in the sounding [*Blanchard*, 1998]. Following earlier studies [e.g., *Lucas et al.*, 1994b], the NCAPE represents the amount of thermodynamic instability in the environment but takes the "shape-of-the-CAPE" into account via the normalization factor. For example, NCAPE = 0.1 J kg^{-1} m^{-1} could be representative of CAPE = 1000 J kg^{-1} distributed over a depth of 10 km (as is common in the Tropics).

The derivations of CAPE and NCAPE incorporate a number of assumptions that have been the subject of debate in the community, e.g., a critical assumption of no mixing between the parcel and the environment. In fact, parcels do entrain a significant amount of ambient air throughout the course of ascent (especially true over tropical oceans where thermal/plume widths are relatively small), and subsequent mixing processes serve to homogenize thermal and moisture perturbations within parcels. Furthermore, there are known moisture biases within the reanalysis product used in this analysis [e.g., *Vesperini*, 2002] that would lead to increasing uncertainty in our calculations. We acknowledge these shortcomings of the chosen data and emphasize that these metrics for thermal instability (CAPE and NCAPE) are only estimates of the potential intensity of deep convection based on the available data. That being said, these data sets are considered the best available to work with in large-scale analyses.

This study emphasizes the role of NCAPE as an estimator for the potential intensity of deep convection. It is possible that NCAPE can be ambiguous in this context because similar values may be found for different thermodynamic environments. For example, the NCAPE computed for a sounding with a shallow layer of positive area with a relatively small value of CAPE may be comparable to the NCAPE in a sounding with a deep layer of positive area and large CAPE. In each case, convection that develops is likely to be very different. When we looked at the distribution of the depth of positive area in each sounding in our data subset, we found a sharp peak in frequency near a depth of 10 km (depths $<$4 km accounted for roughly just 5% of our sample) in line with unstable conditions observed in the tropical atmosphere. The fact that the majority of soundings with NCAPE $>$0 J kg^{-1} m^{-1} in our sample exhibited deep layers of positive parcel buoyancy increased our confidence in using NCAPE as a metric for thermodynamic instability in the investigation.

The LCL was approximated by taking the difference between a parcel's surface temperature and dew-point temperature, and then multiplying by a constant, $c = 0.12$ km K^{-1} [e.g., *Iribarne and Godson*, 1981]. Next, the local height of the 0°C isotherm was estimated by linear interpolation from the nearest neighbor in the ERAi vertical temperature profile. The approximations for the LCL and the local freezing height were found to agree generally well with observations from the global upper-air network. We then calculated the WCD for each CF by finding the vertical distance between the approximate LCL and the freezing level.

The mean vertical profile of radar reflectivity (VPRR) was computed for each CF by cross-referencing the version 7 2A25 attenuation-corrected reflectivity profile [*Iguchi et al.*, 2000]. The geographic centroid of each CF was noted, and the nearest *convective* pixel (according to the version 7 2A23 raintype algorithm) was identified as the reference position (ray and scan indices) within the orbital 2A25 data array. Next, "SEARCH2D" software from the Interactive Data Language (www.exelisvis.com) was used to index array positions that had both convective precipitation and a continuous path of connectivity to the reference position. The angle between the local zenith and the slant path of the radar beam was then used to calculate the height of radar returns in each VPRR using basic trigonometry. The mean VPRR for individual CFs was then computed by taking the mean of the linear reflectivity at indexed array positions (in the horizontal dimensions) at all 80 heights assuming a 250 m interval in the vertical. To mitigate the effects of near-surface ground clutter, we restricted the VPRR to all PR returns above 1.5 km altitude (approximately less than PR range bin 73).

Importantly, the average height of 30 dBZ echoes (AVGHT30) is defined to be the peak altitude in the *mean* VPRR where the reflectivity was between 30.0 and 39.9 dBZ (inclusive). Note, however, that the definition of AVGHT30 differs from the maximum height of 30 dBZ echoes (MAXHT30) in the original CF database since the latter refers to the *single maximum altitude* within a CF where the reflectivity is greater than or equal to 30 dBZ. AVGHT30 takes the area-average behavior of the 30 dBZ echo top height surface into account, whereas MAXHT30 indicates the behavior of the peak(s) of the 30 dBZ echo top height surface (i.e., the single strongest convective pixel/core resolvable with TRMM PR). Lastly, the elevation of the surface

(i.e., the "elev" parameter in the CF data set) has been subtracted, such that AVGHT30 is representative of height relative to the ground surface. By definition, the grouped TRMM PR pixels that constitute a CF contain shallow and deep convective pixels, and we adhere to this standard definition in the current study (as opposed to excluding shallow convective pixels within each CF/LPCF). Therefore, in the computation of mean VPRR and AVGHT30, the presence of shallow convective pixels within the larger CF would tend to offset the contributions from deep convective pixels and possibly weight the 30 dBZ echo height statistics toward lower altitudes.

The CF database algorithm attributes lightning flashes to individual CFs if the flash location falls within the boundary of grouped convective pixels. Total lightning flash rate was estimated by taking the quotient of the flash count and the view time, or the estimated time during which the CF was in LIS's field of view (units of flashes min^{-1}). Total lightning density (TLD) for each CF was then computed by taking the estimated total lightning flash rate and normalizing by the approximate feature area (km^2). While TRMM LIS observations extend from 38°S–38°N, CFs and LPCFs are defined only within the latitudinal limit of the TRMM PR observations, i.e., 36°S-36°N; thus, our results apply to CFs and LPCFs within the domain of TRMM PR observations.

There are multiple potential "noise" sources that could result from the above feature attribution scheme coupled with the TRMM satellite observation strategy. Most importantly, given the myriad of convective scale processes that are not resolved by the relatively coarse thermodynamic and aerosol grids and the impossibility of knowing *exactly* which thermodynamic environments and aerosol concentrations each CF interacts with, scatter about some central value is expected. For example, our preliminary analyses showed that appreciable total lightning flash rates occurred in LPCFs where our scheme attributed the lowest values of NCAPE. It was determined that these LPCFs occurred in the vicinity of large gradients in thermodynamic instability; these LPCFs accounted for a small fraction of the data set (~6% of LPCFs) and were excluded from further analysis due to the uncertainties surrounding their respective thermodynamic environments.

The TRMM satellite has a forward propagation speed of ~7 $\mathrm{km\ s}^{-1}$ such that any CF may be in the instrument field of view for a maximum of ~90 s. Then, it is expected that "snapshot" observations by TRMM PR/LIS will depict CFs at various stages in their respective life cycles in any given orbit—constituting another potential source of variability. Additionally, close inspection of orbital level data from PR/LIS for individual CFs illustrated that larger CFs sometimes have significant lightning observed beyond the PR swath boundary so the radar/lightning correspondence may be compromised. We tried filtering CFs within varying distances from the PR swath edge (cross-track PR pixels 0 and 49) and found that our results were insensitive to this limitation in the data. We chose to include all CFs, regardless of their proximity to swath boundaries, in an effort to maximize the strength of our statistical findings.

Separate data populations of CFs for continental and oceanic regions, both with and without lightning, were simultaneously stratified by the three independent parameters (NCAPE, N40, and WCD) to test various aspects of our hypothesis. The data were first separated by WCD and then the data were binned by N40 and NCAPE using set intervals in order to facilitate comparison between specific environments of interest. A considerable effort went into understanding how WCD varies throughout the tropical/subtropical domain. The probability density functions of WCD were computed at every reanalysis grid point and time step for the 8-year period (regardless of whether there was an overpass by TRMM); the median WCD in the domain of interest was found to be very close to 4200 m. Therefore, discussion of differences with respect to "shallower" and "deeper" WCD in this paper is relative to WCD = 4200 m.

In our examination of VPRR for the global sample of CFs, we investigated the potential impacts of aerosols in fixed background thermodynamic environments. It is difficult to rigorously define pristine and polluted aerosol environments between continents and oceans since the underlying aerosol distributions are so different [e.g., *Williams et al.*, 2002, and references therein]. For this reason, we introduce stratifications for the range from pristine to heavily polluted environments (N40 $<$100, 100–200, 200–500, and $>$500 cm^{-3}) based on the cumulative probability distribution function for the global population. We use average 30 dBZ echo top height (AVGHT30), TLD, and VPRR as proxies for the variability of convective intensity throughout the Tropics in the following investigation [e.g., *Zipser et al.*, 2006, and many others].

Table 1. Census of CFs and LPCFs[a]

Domain	CFs	LPCFs	CFs (AVGHT30 >5 km)	LPCFs (AVGHT30 >5 km)
Global	12,232,564	503,133	1,457,919	263,378
Continents	2,148,492	360,190	388,859	162,593
Oceans	10,084,072	142,943	1,069,060	100,785

[a]Populations of convective features (CFs) and lightning-producing convective features (LPCFs; i.e., CFs with lightning flash rates above TRMM LIS's minimum detection threshold) over the TRMM domain for the years 2004–2011. The first two columns represent populations in the original CF/LPCF database, while the latter two columns represent the sample sizes of the data subset for the current analysis.

3. Results

3.1. Global Climatology

Roughly 12.2 million CFs were observed by the TRMM satellite between 2004 and 2011, but we decided to include only CFs and LPCFs with (1) AVGHT30 >5 km and (2) with collocated aerosol and thermodynamic variables within the upstream swath in our final data subset. The choice to truncate the data to CFs/LPCFs with AVGHT30 >5 km reduced our data subset to just under 1.5 million CFs (~260,000 LPCFs; see Table 1 for a sample sizes of each population). However, by this method, we attempt to isolate quasi-upright, deep convective features since we expect shallow and deep CFs to respond differently to perturbations to environmental thermodynamics and aerosol concentrations [e.g., *Tao et al.*, 2012; *Rosenfeld et al.*, 2014]. We then binned these populations of CFs and LPCFs in the 8-year temporal subset geographically on a 1° grid and produced global distributions of CF/LPCF frequency, mean AVGHT30, mean TLD, and mean distributions of NCAPE, N40, and WCD for both CFs (Figures 1a–1e) and LPCFs (Figures 1f–1j).

Globally, the frequency of deep CFs maximizes in the Intertropical Convergence Zone and over the western Pacific Ocean (Figure 1a). Deep CFs are nearly absent from subsidence regions on the eastern periphery of major ocean basins. The global distribution of AVGHT30 for the subset of deep CFs (Figure 1b) shows heights of <6 km over oceans and 6 km to more than 7 km over continents in the Tropics and subtropics on average. These differences generally agree with the spatial variability of lightning shown in Figure 1g, but the strength of correlation between these two fields appears to vary between continents and oceans. The maxima in the AVGHT30 distribution occur over the Sahel, Southern Great Plains of the United States, in lee of the central Andes Mountains, and over parts of northwest India. Notably, the distributions of MAXHT30 for LPCFs (and, to some extent, for CFs) in our data subset show roughly similar values, ~9 km, between continents and oceans over much of the TRMM domain (not shown). The homogeneity of the MAXHT30 climatology for LPCFs coupled with the striking land-ocean contrast in TLD constitutes an important set of findings and will be discussed in a subsequent section.

In agreement with previous studies, the frequency of LPCFs over continents is consistently an order of magnitude larger than the frequency of LPCFs over ocean (Figure 1f). However, the vast majority of CFs (including CFs without lightning) occurs over ocean (cf. Table 1). CFs with lightning flash rates above LIS's minimum detection threshold (~0.7 flashes min^{-1}) represent only a small fraction of the total number of CFs observed (approximately 3.4% of CFs observed by the TRMM satellite between 2004 and 2011). Although LPCFs in our data subset account for a small fraction of the full CF database, prominent aspects of the general circulation like the Intertropical and South Pacific Convergence Zones, the African Easterly Jet, and midlatitude storm tracks are readily noticeable in Figure 1f as these areas are favorable for the development of deep convective clouds.

The annual mean distribution of TLD (Figure 1g) depicts the strong climatological land-ocean contrast in lightning that has been previously documented [*Christian et al.*, 2003]. TLD over continents is greater than TLD over ocean by a factor of 2–5. While intense convection capable of producing copious lightning does occur over remote tropical oceans [e.g., *Kelley et al.*, 2010], Figure 1f shows that such convection occurs very infrequently compared to continental areas. Abrupt decreases in TLD near coastlines are also shown in Figure 1g in agreement with previous global lightning climatologies.

In general, the difference in NCAPE between continental and oceanic regions across the TRMM domain for both CFs and LPCFs is small in the annual mean sense (Figures 1c and 1h). At first, this result was surprising given the emphasis on the importance of thermal instability in moist convective processes in the literature to date.

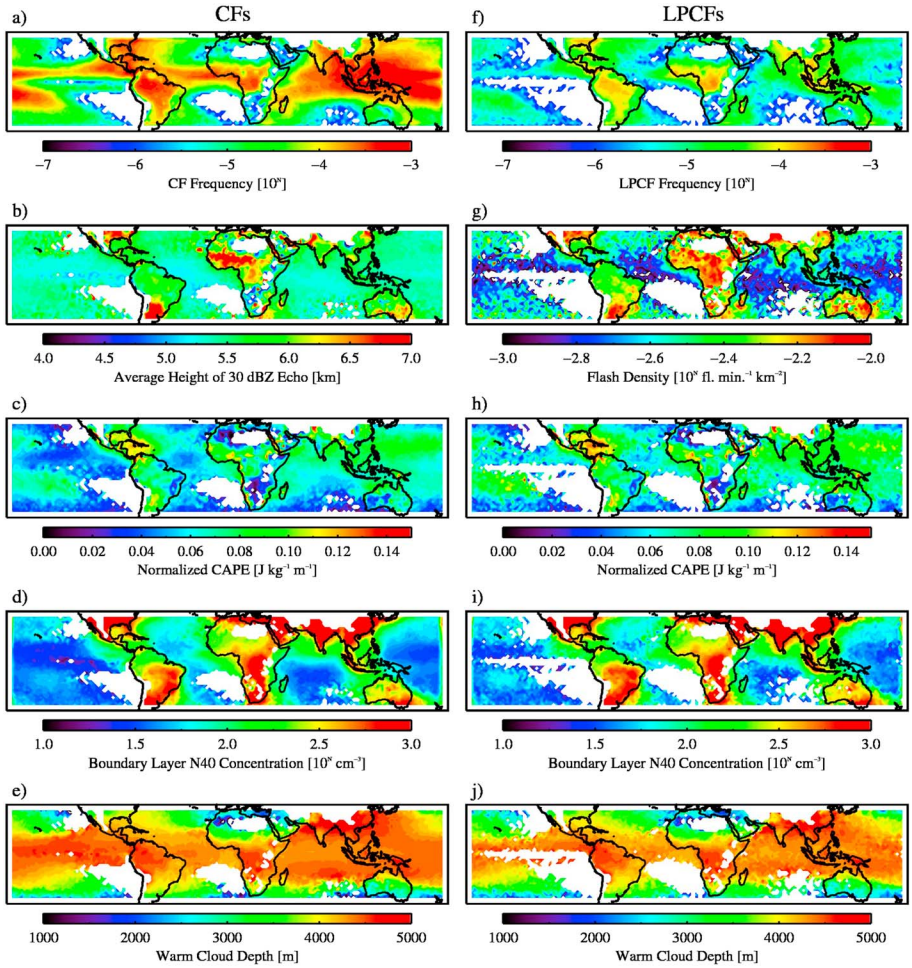

Figure 1. Annual mean distributions of (a) CF frequency, (b) AVGHT30, (c) NCAPE for CFs, (d) N40 for CFs, (e) WCD for CFs, (f) LPCF frequency, (g) TLD, (h) NCAPE for LPCFs, (i) N40 for LPCFs, and (j) WCD for LPCFs averaged over 1° grid boxes between 38°S and 38°N for the years 2004–2011 (*see text for definitions*). CFs (LPCFs) with AVGHT30 >5 km (with flash rates above the minimum detection threshold of the TRMM lightning imaging sensor) were analyzed (both constraints in the case of LPCFs).

However, several researchers have argued that the difference in conditional instability between continents and oceans in the tropics is small on average [e.g., *Williams and Renno*, 1993; *Lucas et al*., 1994a, 1994b], consistent with the results found here. The annual mean distributions of the depth of the positive area (i.e., the normalization factor in the NCAPE computation) in a given sounding depict general longitudinal homogeneity (depth ~10 km) and general decreases in the poleward direction (not shown). The differences in the distributions of NCAPE for CFs (Figure 1c) and NCAPE for LPCFs (Figure 1h) are not readily discernible, but will be discussed in more detail below.

The annual distributions of boundary layer N40 for CFs and LPCFs in Figures 1d and 1i are consistent with observations of an order-of-magnitude difference in the mean aerosol concentrations between continents and oceanic regions. The most pristine environments are the equatorial regions of the Pacific and Indian Oceans with mean N40 values near a few 10s cm^{-3}. Globally, N40 is maximized over continental regions in developing counties and in areas where seasonal biomass burning takes place (e.g., central equatorial Africa and the southern/southeastern portions of the Amazon). Several oceanic regions are subject to offshore aerosol transport as evidenced by N40 reaching as high as a few hundred per cubic centimeter (e.g., downstream of the eastern United States, South America, South Africa, and eastern Australia).

The global distributions of WCD (Figures 1e and 1j) show considerable homogeneity in the deep Tropics. The greatest distance between the freezing level and LCL, on average, is found over parts of the Amazon,

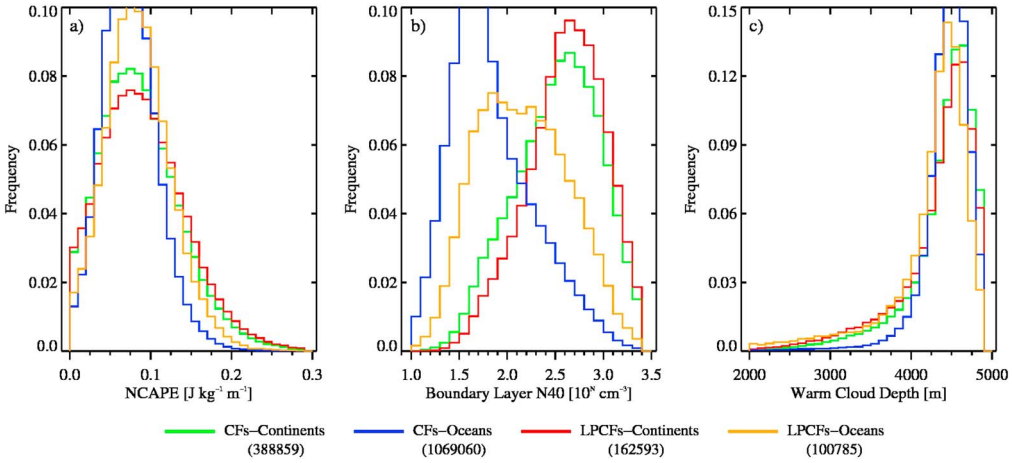

Figure 2. Probability density functions of (a) NCAPE, (b) N40, and (c) WCD for CFs over continents (green), CFs over oceans (blue), LPCFs over continents (red), and LPCFs over oceans (orange). The number of CFs or LPCFs is provided in parentheses for each population. CFs (LPCFs) with AVGHT30 >5 km (with flash rates above the minimum detection threshold of the TRMM lightning imaging sensor) were analyzed (both constraints in the case of LPCFs).

equatorial Africa, Southeast Asia, and the Indian and Pacific Oceans for both of the populations of CFs and LPCFs. The fact that WCD generally decreases with increasing latitude is likely due to decreases in boundary layer moisture and the lowering of the local freezing level. Zonal heterogeneity of WCD is most pronounced in the northern hemisphere over continents (e.g., between the United States, northern Africa, and Southeast Asia).

Probability density functions for NCAPE, N40, and WCD for the populations of CFs and LPCFs over both continents and oceans are presented in Figure 2. The median NCAPE for CFs (for LPCFs) is 0.08 J kg^{-1} m^{-1} (0.09 J kg^{-1} m^{-1}) over continents and 0.07 J kg^{-1} m^{-1} (0.08 J kg^{-1} m^{-1}) over oceans. While the distributions of NCAPE (Figure 2a) peak near 0.08 J kg^{-1} m^{-1} for each population of CFs and LPCFs, there is a tendency for CFs over continents and LPCFs to develop in environments with higher NCAPE more frequently.

There are distinct differences between the distributions of N40 for CFs and LPCFs over continents and oceans. Figure 2b shows that CFs over oceans develop in environments that are most frequently characterized by N40 <100 cm^{-3}. In contrast, the distribution of N40 for CFs that develop over continents peaks around 300–500 cm^{-3}. LPCFs over oceans develop in environments with N40 values that are intermediate between those values typical for oceanic and continental CFs. Lastly, the distribution of N40 for LPCFs over continents peaks at approximately 300–500 cm^{-3}; however, the relative frequency of occurrence of LPCFs over continents in heavily polluted environments (N40 >1000 cm^{-3}) is higher than that for any other subset of the total CF population considered.

The distributions of WCD for CFs and LPCFs (Figure 2c) each peak near 4500 m (slightly deeper than the global median value computed from all reanalysis time steps), and there is a subtle tendency for LPCFs over continents and oceans to occur more frequently at shallower WCD when compared to the relative frequency of occurrence for the populations of CFs over continents and oceans. It is also apparent that there are relatively few observations of WCD shallower than 2000 m in our data subsets, and therefore, we limit the analysis to WCD between 2000 and 5000 m.

While the global climatological and probability distributions in Figures 1 and 2 lend physical credence to the behavior of each variable, they only allow for qualitative characterization of potential relationships between proxies for convective intensity and NCAPE, N40, and WCD. Furthermore, these climatological distributions support the idea that the variability in TLD and AVGHT30 could result from some combination of NCAPE, N40, and WCD. We now turn to a discussion of this topic.

3.2. Three-Parameter Stratification: Total Lightning Density and Average Height of 30 dBZ

We begin our discussion by examining the relationships between NCAPE, N40, WCD, and TLD. For the global population of LPCFs, we find that TLD increases from <0.0014 up to 0.01 fl. min^{-1} km^{-2} (a 600% increase)

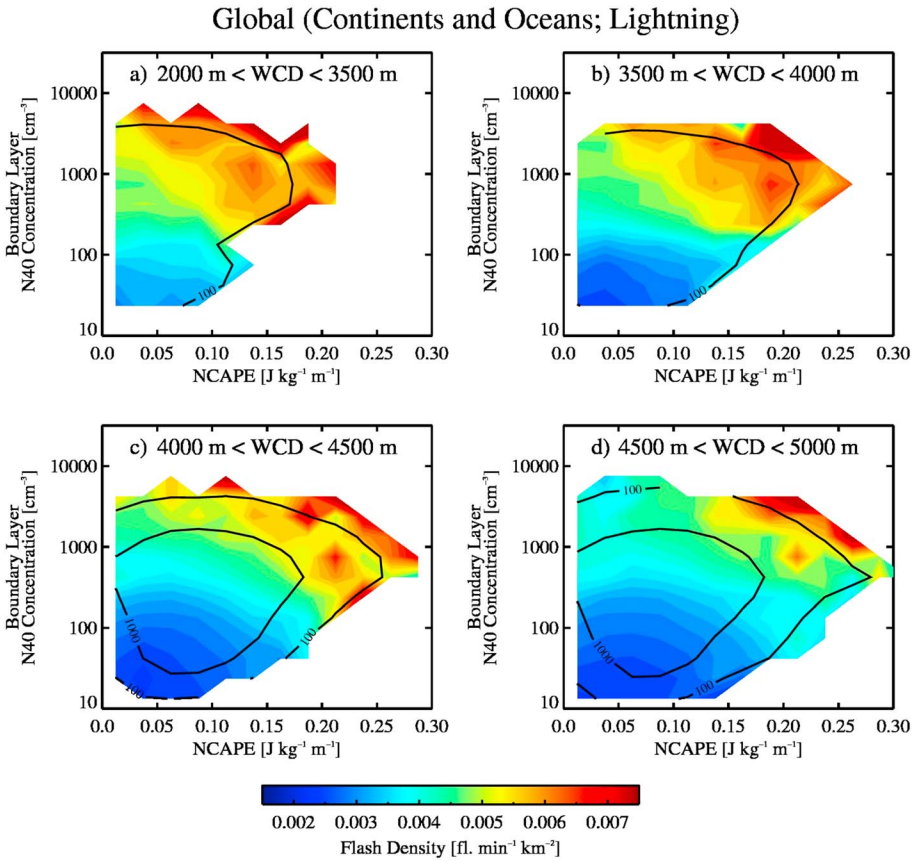

Figure 3. Total lightning density (TLD; shaded) plotted as a two-dimensional function of NCAPE and N40 for CFs across the global TRMM domain (continents and oceans) for (a) 2000 m < WCD ≤ 3500 m, (b) 3500 m < WCD ≤ 4000 m, (c) 4000 m < WCD < 4500 m, and (d) 4500 m < WCD < 5000 m. Black solid contours indicate the number of observations in each bin within the parameter space. LPCFs with flash rates above the minimum detection threshold of the TRMM lightning imaging sensor and AVGHT30 >5 km were analyzed. A threshold of 20 LPCFs was set for a given bin before the output was plotted.

with *both increasing N40 and NCAPE for all simultaneous stratifications of WCD* (Figures 3a–3d). Additionally, the highest TLD occurs for N40 $>1000\,cm^{-3}$ and NCAPE $>0.15\,J\,kg^{-1}\,m^{-1}$, while the lowest TLD is generally found below N40 $<500\,cm^{-3}$ and NCAPE $<0.15\,J\,kg^{-1}\,m^{-1}$ for all WCD stratifications. Finally, as WCD trends from shallower (Figure 3a) to deeper (Figure 3d), the highest median values of TLD become restricted to higher values of both NCAPE and N40, suggesting a modulation of the NCAPE-N40-TLD relationship by WCD. Figure 3 also illustrates important conditional or partial sensitivities of TLD to NCAPE and N40 (e.g., changes in TLD along a constant vertical/horizontal parameter space trajectory holding other variables constant). The partial sensitivity of TLD with respect to changes in NCAPE and N40 is systematically detailed in section 3.3 below.

Next, we examined the response of AVGHT30 in the population of CFs with AVGHT30 >5 km (shallow CFs, i.e., features with AVGHT30 <5 km, were excluded). The distributions of AVGHT30 for these CFs in response to NCAPE and N40 for simultaneous stratifications of WCD (Figures 4a–4d) are broadly consistent with the results shown in Figure 3. AVGHT30 increases from 5.25 up to more than 7.5 km as both NCAPE and N40 increase, with the peak AVGHT30 found for N40 $>1000\,cm^{-3}$ and NCAPE $>0.15\,J\,kg^{-1}\,m^{-1}$ while minima are found for N40 $<500\,cm^{-3}$ and NCAPE $<0.15\,J\,kg^{-1}\,m^{-1}$ for all WCD stratifications. Analogous to Figure 3, there are again aspects of the two-dimensional dependence of AVGHT30 on NCAPE and N40, i.e., partial sensitivities, and these sensitivities will be discussed in section 3.3 below.

Our next objective was to determine whether the response of these proxy measures for convective intensity varies for CFs/LPCFs between continents and oceans. From climatology in Figure 1, LPCFs occur predominantly

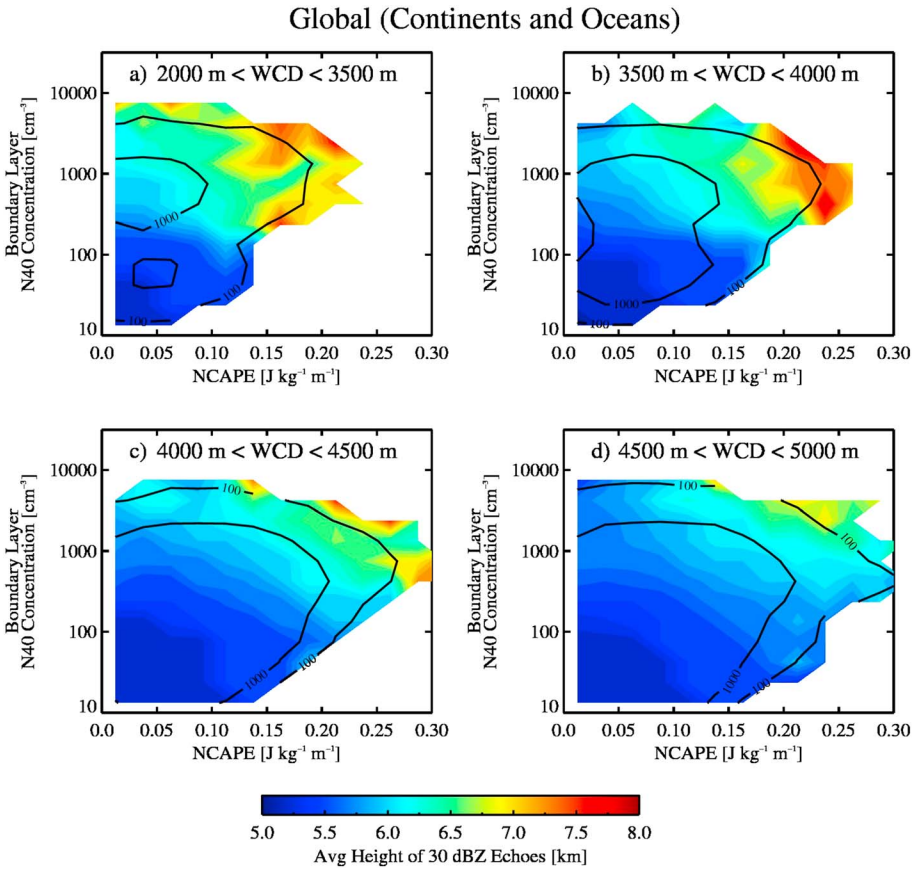

Figure 4. As in Figure 3 but for the average height of 30 dBZ echoes (AVGHT30; shaded). CFs with AVGHT30 >5 km were analyzed. A threshold of 20 CFs was set for a given bin before the output was plotted.

over continents. On average, TLD is greater and AVGHT30 is higher over continents compared to oceanic regions. LPCFs over continents and oceans are shown to populate different sections of the NCAPE-N40 parameter space (Figure 5); LPCFs over continents occur in more polluted environments across a wide range of NCAPE values, while LPCFs over oceans occur in environments with lower NCAPE and generally low aerosol number concentrations. Here we present only the extremes of the WCD stratifications in our sample to illustrate potential variability with respect to shallower and deeper WCD. Do the differences in the intrinsic properties of the environments for continental and oceanic CFs impact the resulting sensitivities of lightning and radar quantities to NCAPE and N40?

Over continents for shallower WCD (Figure 5a), TLD is shown to increase from about 0.0033 up to more than 0.012 fl. min^{-1} km^{-2} (a 268% increase) as NCAPE and N40 increase together. Over oceans for shallower WCD (Figure 5b), TLD increases from approximately 0.0018 up to 0.006 fl. min^{-1} km^{-2} (roughly a 300% increase) as NCAPE and N40 simultaneously increase for fixed WCD. For deeper WCD (Figures 5c and 5d), TLD increases by roughly 300–400% again as both NCAPE and N40 increase simultaneously. In all cases (both shallower and deeper WCD), the minimum TLD is found for NCAPE $<0.10\,J\,kg^{-1}\,m^{-1}$ and N40 $<500\,cm^{-3}$ and the maximum TLD is generally found for NCAPE $>0.15\,J\,kg^{-1}\,m^{-1}$ and N40 $>1000\,cm^{-3}$.

We conducted a similar analysis for the sensitivity of AVGHT30 over continents and oceans, and the results for shallower and deeper WCD are shown in Figure 6. Over continents (Figures 6a and 6c), AVGHT30 increases from approximately 5.5 to 8.0 km for shallower WCD and approximately 5.25 to 7.25 km for deeper WCD as NCAPE and N40 increase simultaneously. Over oceanic regions for shallower and deeper WCD (Figures 6b and 6d), AVGHT30 increases from roughly 5.25 to 6.75 and 5.25 to 6.25 km, respectively, as both NCAPE and N40 increase, with the maximum values of AVGHT30 found for NCAPE $>0.10\,J\,kg^{-1}\,m^{-1}$ and N40 ~$1000\,cm^{-3}$. The minimum values of AVGHT30 are again found for low NCAPE and low N40.

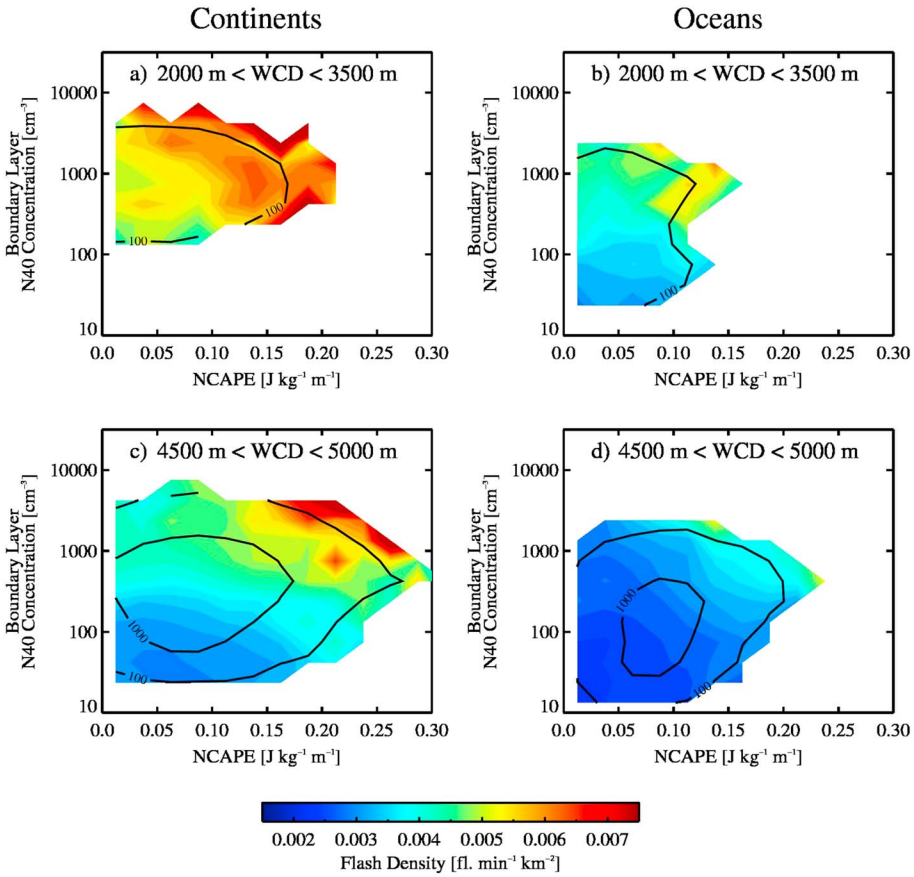

Figure 5. Total lightning density (TLD; shaded) plotted as a two-dimensional function of NCAPE and N40 for LPCFs over (left) continents and (right) oceans for (a and b) 2000 m < WCD ≤ 3500 m and (c and d) 4500 m < WCD < 5000 m. Black solid contours indicate the number of observations in each bin within the parameter space. LPCFs with flash rates above the minimum detection threshold of the TRMM lightning imaging sensor and AVGHT30 >5 km were analyzed. A threshold of 20 LPCFs was set for a given bin before the output was plotted.

Together, the results for the sensitivity of TLD and AVGHT30 with respect to NCAPE and N40 simultaneously over continents and oceans are consistent with the behavior observed for the global populations of CFs and LPCFs (Figures 3 and 4). Furthermore, the variability of AVGHT30 over continents and oceans mirrors the response of TLD to combinations of NCAPE/N40 for fixed WCD, emphasizing potential correlation between 30 dBZ radar reflectivity and lightning characteristics in convective features (analysis of the relationship between lightning and 30 dBZ radar reflectivity will be provided in a subsequent section).

3.3. Partial Sensitivity of TLD/AVGHT30 to NCAPE and N40

To this point, we have focused on the sensitivity of lightning and radar reflectivity to simultaneous changes in NCAPE and N40. However, it is important to explore how the response of deep convection varies with respect to individual predictor variables with other factors held fixed. Hence, we focus on partial sensitivities of TLD/AVGHT30 (e.g., ΔAVGHT30/ΔNCAPE) and how the magnitudes of these terms compare to the observed total response of TLD/AVGHT30 to simultaneous changes in NCAPE and N40 presented in section 3.2. The partial sensitivities of proxy variables (i.e., TLD and AVGHT30) with respect to NCAPE have been plotted for fixed N40 above and below the median value of N40 over the global domain, over continents, and over oceans (for shallower and deeper WCD). Likewise, the relationships between TLD and AVGHT30 with respect to N40 are plotted for fixed NCAPE above and below the median value of NCAPE for shallower and deeper WCD for the global domain, over continents, and over oceans (Figures 7 and 8). The partial sensitivity of TLD and AVGHT30 with respect to WCD was also examined; these results will be detailed in section 3.4 below.

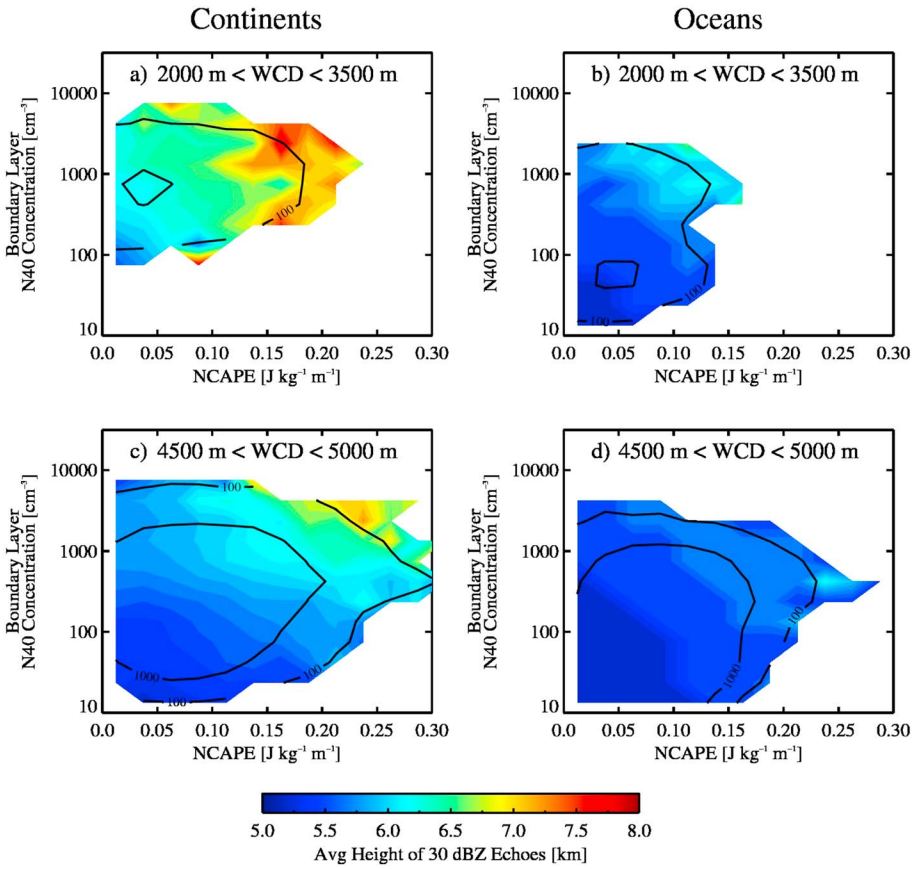

Figure 6. As in Figure 5 but for the average height of 30 dBZ echoes (AVGHT30; shaded). CFs with AVGHT30 >5 km were analyzed. A threshold of 20 CFs was set for a given bin before the output was plotted.

First, we present the partial sensitivity of TLD as functions of NCAPE and N40 holding other independent variables fixed (Figure 7). Note that there was a minimum threshold of 20 LPCFs required before the bin median was plotted in each case; error bars represent the interquartile range in each bin. The average range of the relationship between TLD and each predictor variable (e.g., NCAPE and N40) for the global domain, for continents, and for oceans are 104%, 62%, and 172% with respect to NCAPE (Figures 7a–7c) and 322%, 168%, and 168% with respect to N40 (Figures 7d–7f). The range of the individual relationships described above are given in Table 2 for reference. Next, in the legend of each panel, we provide the linear correlation between NCAPE and N40 for each stratification in an effort to address the possibility of the trends being the result of simultaneous correlation. For all stratifications over the global domain, over continents, and over oceans, the linear correlation is generally smaller than 0.20, suggesting that NCAPE and N40 are approximately independent in each case and that variations in the predictand are more likely attributable to the changes in the abscissa.

From Figure 7, it is clear that the average ranges of variability in TLD with respect to N40 over the global domain and over continents are larger when compared to the sensitivity with respect to NCAPE (the behavior of TLD over oceans being the exception). Furthermore, TLD is greater at a given value of NCAPE when N40 is above the median value (true for both shallower and deeper WCD). Additionally, the slope of the relationship between TLD and NCAPE remains roughly constant for the different stratifications of N40 and WCD (Figures 7a–7c), while there is a considerable amount of variability in the slope of the relationship between TLD and N40 for different stratifications of NCAPE and WCD (Figures 7d–7f). The steepest slope in the latter cases is found for NCAPE above the median value and shallower WCD, and the smallest slope is found for low NCAPE and deeper WCD. The slope for the TLD versus N40 relationship, specifically for low NCAPE and deeper WCD, diminishes and becomes negative beyond N40 $>1000\,\mathrm{cm}^{-3}$;

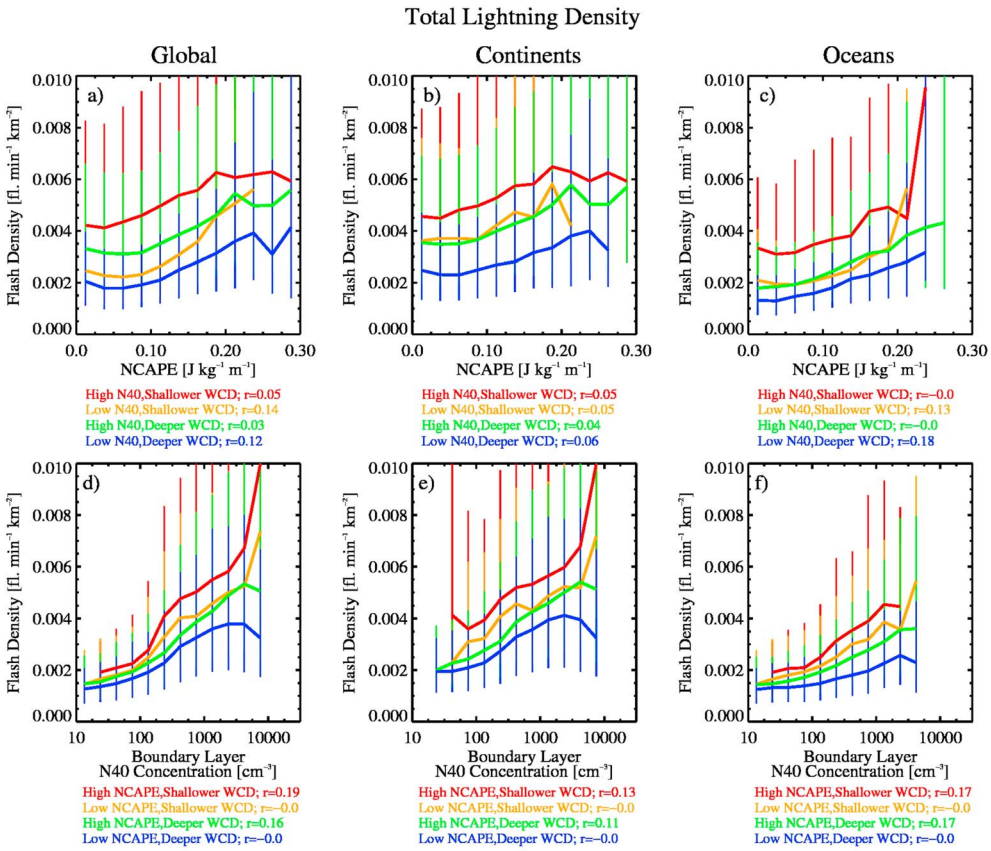

Figure 7. The partial sensitivity of total lightning density (TLD) with respect to (a–c) NCAPE and with respect to (d–f) N40 for LPCFs (left) over the global TRMM domain, (center) over continents, and (right) over oceans (*see text for definition of individual stratifications*). Medians of TLD are plotted, and the interquartile range in each bin is represented by the error bars. The linear correlation, *r*, between NCAPE and N40 within each data subset is provided in each panel's legend. LPCFs with flash rates above the minimum detection threshold of the TRMM lightning imaging sensor and AVGHT30 >5 km were analyzed. A threshold of 20 LPCFs was set for a given bin before the output was plotted.

this result agrees with the changes in lightning behavior with respect to aerosols that were observed by *Altaratz et al*. [2010] during four dry seasons over the Amazon.

Decreasing TLD with increasing N40 (N40 $>1000\,cm^{-3}$) is consistent with earlier hypotheses put forth in the literature—that the combined effects of a reduction in conditional instability (as a consequence of aerosol absorption/diminished shortwave fluxes at the surface) and increased water loading (owed to reduced coalescence) in ascending parcels reduce updraft intensity for aerosol concentrations beyond some optimum value. The observed behavior of TLD for high N40 (N40 $>1000\,cm^{-3}$) is consistent with a decrease in riming efficiency as cloud droplets become small enough under high aerosol concentrations to yield an overall decrease in the collision efficiency with graupel particles [e.g., R08; *Storer and van den Heever*, 2013].

We also examined the partial sensitivity of AVGHT30 with respect to changes in NCAPE (Figures 8a–8c) and N40 (Figures 8d–8f) in a similar manner, and the results were found to be largely consistent with what was shown for TLD in Figure 7. The average ranges of the AVGHT30 versus NCAPE relationship (holding N40 and WCD fixed) were 0.89, 0.77, and 0.75 km for the global domain, continents, and oceans, respectively (statistics for individual relationships are listed in Table 2). By comparison, the average ranges of the relationship between AVGHT30 and N40 (holding NCAPE and WCD constant) were 1.14, 0.94, and 0.81 km. Thus, the average ranges in AVGHT30 with respect to N40 are slightly larger than the ranges in AVGHT30 with respect to NCAPE over the global domain and continents, and over oceans. Again, we find that AVHT30 is higher at a given value of NCAPE when N40 is above the global median (for fixed WCD; Figures 8a–8c) and AVGHT30 levels off or begins decreasing slightly for values of N40 $>1000\,cm^{-3}$ (e.g., Figures 8d–8f). Although the linear correlations between NCAPE and N40 in each stratification of AVGHT30 (in the legend of

Table 2. Partial Sensitivities of AVGHT30 and TLD[a]

Partial Sensitivity	Global	Continents	Oceans
$\left[\frac{\Delta AVGHT30}{\Delta N40}\right]_{NCAPE\ Low}$	(+1.26 km/+0.69 km)	(+1.01 km/+0.65 km)	(+0.75 km/+0.25 km)
$\left[\frac{\Delta AVGHT30}{\Delta N40}\right]_{NCAPE\ High}$	(+1.49 km/+1.13 km)	(+1.11 km/+1.00 km)	(+1.00 km/+1.25 km)
$\left[\frac{\Delta AVGHT30}{\Delta NCAPE}\right]_{N40\ Low}$	(+0.75 km/+0.68 km)	(+0.62 km/+0.47 km)	(+0.50 km/+0.25 km)
$\left[\frac{\Delta AVGHT30}{\Delta NCAPE}\right]_{N40\ High}$	(+1.38 km/+0.76 km)	(+1.28 km/+0.71 km)	(+1.50 km/+0.75 km)
$\left[\frac{\Delta TLD}{\Delta N40}\right]_{NCAPE\ Low}$	(+408%/+199%)	(+211%/+112%)	(+276%/+106%)
$\left[\frac{\Delta TLD}{\Delta N40}\right]_{NCAPE\ High}$	(+421%/+263%)	(+178%/+171%)	(+138%/+150%)
$\left[\frac{\Delta TLD}{\Delta NCAPE}\right]_{N40\ Low}$	(+153%/+131%)	(+61%/+74%)	(+193%/+145%)
$\left[\frac{\Delta TLD}{\Delta NCAPE}\right]_{N40\ High}$	(+53%/+80%)	(+45%/+66%)	(+209%/+141%)

[a]Partial sensitivities of AVGHT30 (km) and TLD (%) with respect to NCAPE and N40 for (shallower/deeper) WCD for CFs/LPCFs over the global domain, over continents, and over oceans. Each value represents the max range of the one-dimensional comparisons in Figures 7 and 8; the first value is the change when WCD is shallower and the second value is the change when WCD is deeper (see text for stratification methodology).

each panel in Figure 8) are slightly larger compared with the values for the stratifications of TLD, the *r* values remain below about 0.25, again lending to the idea that NCAPE varies approximately independently of N40.

For CFs with and without lightning across the global Tropics, the resulting partial sensitivities of both TLD and AVGHT30 to NCAPE and N40 (for fixed WCD) support the hypothesis that aerosols modulate the amount of

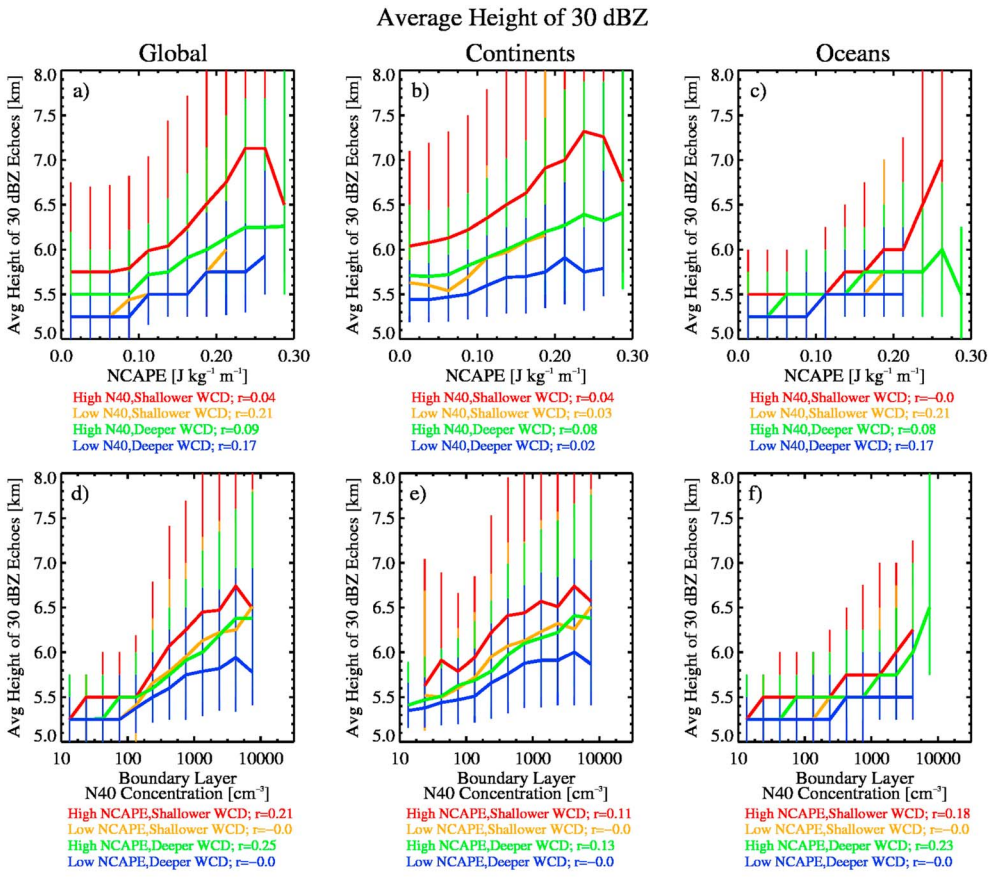

Figure 8. As in Figure 7 but for the partial sensitivity of the average height of 30 dBZ echoes (AVGHT30). CFs with AVGHT30 >5 km were analyzed. A threshold of 20 CFs was set for a given bin before the output was plotted.

conditional instability realized by ascending parcels (e.g., R08). TLD (AVGHT30) was found to be greater (higher) when NCAPE increased in the presence of higher aerosol concentrations (e.g., Figures 7a–7c and 8a–8c), and the slope of both the TLD versus N40 and AVGHT30 versus N40 relationships decreased to zero and became negative for N40 $>1000\,cm^{-3}$ (e.g., Figures 7d–7f and 8d–8f). We emphasize that the average ranges of the TLD/AVGHT30 versus NCAPE and N40 relationships separately amounted to a fraction of the total changes that were observed above in section 3.2. Therefore, our results suggest that (1) both NCAPE and N40 are important factors that contribute to the development of high TLD and AVGHT30 in our data subsets and (2) there may be other factors that are simultaneously influencing these attributes of deep convection.

3.4. The Importance of Warm Cloud Depth

In the above discussion, the sensitivity of lightning and radar reflectivity to simultaneous changes in NCAPE and N40 as well as partial sensitivities of these quantities to NCAPE and N40 holding other independent variables constant was shown to be appreciable. However, our results illustrate considerable variability in both TLD and AVGHT30 with respect to WCD. In Figure 9, we show the difference in TLD and AVGHT30 between shallower WCD (WCD <4200 m) and deeper WCD (WCD >4200 m) populations at each point in the NCAPE-N40 parameter space for CFs and LPCFs in the global TRMM domain, over continents, and over oceans, respectively. In each case presented, differences in TLD (percent differences; left panel) and AVGHT30 (height differences; right panel) with respect to WCD are mostly positive—LD is greater and AVGHT30 is higher when WCD is shallower as opposed to deeper. We note that there is an exception for AVGHT30 over continents for low N40 across a range of NCAPE; it is likely that this behavior results from seasonal and regional dependence, i.e., CFs occurring in select regions or preferred times of year (to be discussed in section 4).

We investigated the significance of the differences between populations of TLD or AVGHT30 between shallower and deeper WCD at each NCAPE/N40 point using a Wilcoxon rank-sum test. In context, the Wilcoxon rank-sum test assumes the null hypothesis that the medians of the populations of TLD or AVGHT30 for shallower and deeper WCD are equal. The maximum increase in TLD (Figure 9, left) with respect to WCD at a given NCAPE-N40 point was found to be +91% for the global domain, +86% over continents, and +42% over oceans, and these differences were all significant at the $P = 0.05$ level (i.e., these results were in favor of rejecting the null hypothesis at the 5% level). The maximum positive increases for TLD for the global domain and continents (oceans) occurred for NCAPE $>0.25\,J\,kg^{-1}\,m^{-1}$ and N40 $>1000\,cm^{-3}$ (NCAPE $>0.1\,J\,kg^{-1}\,m^{-1}$ and N40 $>500\,cm^{-3}$). Negative differences in TLD with respect to changing WCD were very small (less than 1%) and were relatively rare. The maximum increase in AVGHT30 (Figure 9, right) with respect to WCD was +1.46 km for the global TRMM domain, +1.19 km over continents, and +1.00 km over oceans, and these differences were also significant at the $P = 0.05$ level. The maximum positive increases of AVGHT30 over both the global domain and over continents (over oceans) occur for NCAPE $>0.2\,J\,kg^{-1}\,m^{-1}$ and N40 $>1000\,cm^{-3}$ (NCAPE $>0.08\,J\,kg^{-1}\,m^{-1}$ and N40 $>1000\,cm^{-3}$).

These results suggest that deep convection in the Tropics is stronger when WCD is shallower since similar responses are noted for both proxies for convective intensity (i.e., TLD and AVGHT30). Additionally, the differences in TLD and AVGHT30 with respect to progressively shallower WCD are largest when NCAPE and N40 are high. In other words, in environments with deeper WCD, higher NCAPE and N40 appear to be necessary to "invigorate" a convective updraft during ascent through the cloud's warm phase.

3.5. Radar Reflectivity/Lightning Correspondence and Sensitivity

Our results indicate that both TLD and AVGHT30 behave similarly in response to changes in both N40 and NCAPE for different stratifications of WCD. Meanwhile, previous studies have documented strong correspondence between radar reflectivity and lightning in many regions [e.g., *Dye et al*., 1989; *Rutledge et al*., 1992; *Petersen et al*., 1996; *DeMott and Rutledge*, 1998; *Petersen and Rutledge*, 2001; *Liu et al*., 2012; *Stolz et al*., 2014]. The climatologies for TLD and AVGHT30 presented above (Figure 1) corroborate the findings of these previous studies; however, our study allows for an attempt to quantify the correspondence between reflectivity and lightning proxies for convective intensity on the global scale. Specifically, we question whether the relationship between TLD and AVGHT30 varies as a function of NCAPE, N40, and/or WCD.

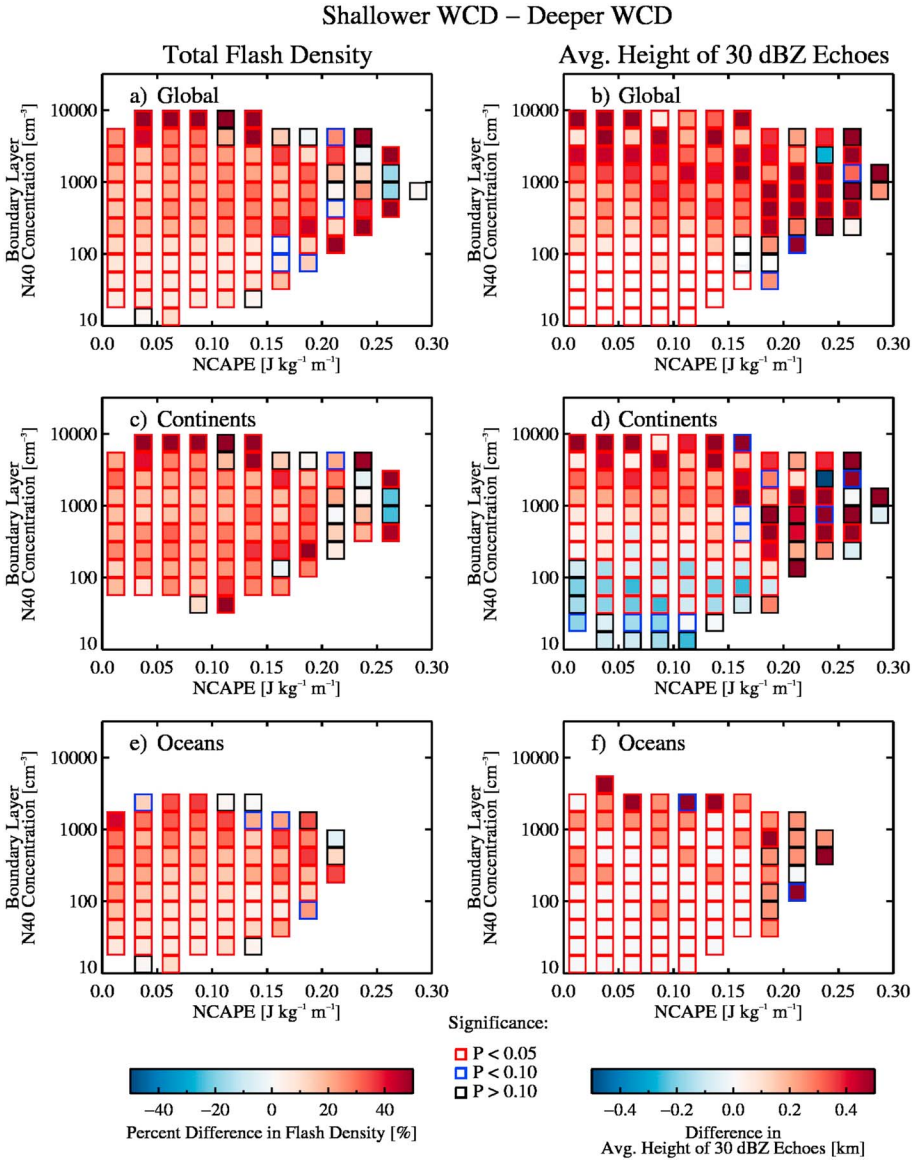

Figure 9. (left) Differences in total lightning density (TLD) and (right) the average height of 30 dBZ echoes (AVGHT30) between shallower WCD (WCD <4200 m) and deeper WCD (WCD >4200 m) for (a and b) the global population of LPCFs and CFs, (c and d) LPCFs and CFs over continents, and (e and f) LPCFs and CFs over oceans for a fixed NCAPE/N40 point. Shading indicates the percent difference in total lightning density and the difference in AVGHT30 in the left and right panels, respectively. Colored outlines for each point in the two-dimensional parameter space illustrate the significance of the difference determined by a Wilcoxon rank-sum test for the difference of medians. CFs (LPCFs) with AVGHT30 >5 km (with flash rates above the minimum detection threshold of the TRMM lightning imaging sensor) were analyzed (both constraints in the case of LPCFs).

Note that this comparison is only possible for deep CFs that produce lightning, and therefore, we were limited to analyzing only 2.1% of the total CF population observed by TRMM during 2004–2011 (i.e., those features with lightning above the minimum detection threshold of TRMM LIS and AVGHT30 >5 km). For this subset of CFs, when TLD is binned by AVGHT30 for a continuum of stratifications of N40 (Figure 10) and the resulting bin medians are plotted, a strong positive relationship is readily apparent ($r = 0.95$–0.98). However, the sensitivity of the TLD versus AVGHT30 relationship decreases with decreasing N40, suggesting that for convective clouds developing in pristine environments, the 30 dBZ reflectivity column has to be deeper in order to produce the same flash density. Evidence of this phenomenon in the continental subset of LPCFs (Figure 10b) is subtle but is more apparent for the oceanic subset of LPCFs

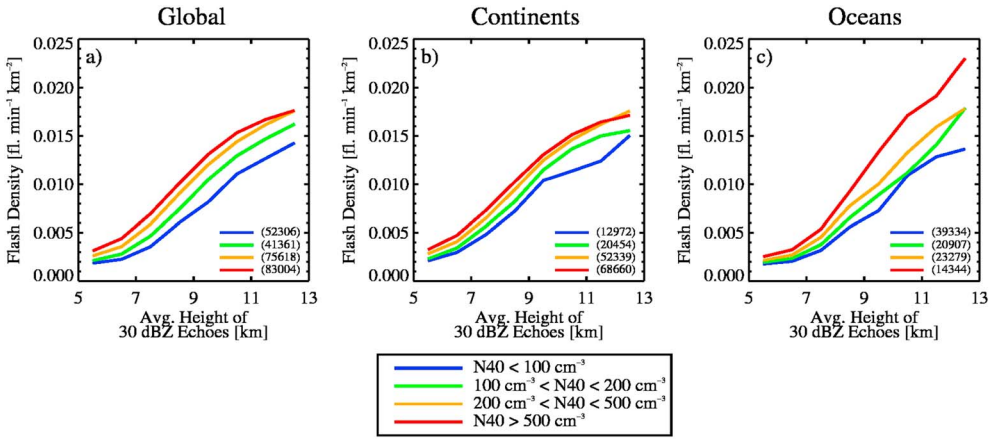

Figure 10. Total lightning density (TLD) versus average height of 30 dBZ echoes for various aerosol stratifications (see legend) for (a) the global population of LPCFs, (b) LPCFs over continents, and (c) LPCFs over oceans. LPCFs with flash rates above the minimum detection threshold of the TRMM lightning imaging sensor and AVGHT30 >5 km were analyzed. A threshold of 20 LPCFs was set for a given bin before the output was plotted. The number of LPCFs in each respective aerosol stratum is provided in parentheses in the lower right corner of each plot.

(Figure 10c). Importantly, this finding points to the possibility of different microphysical properties of the mixed phase region in a convective cloud under different background aerosol concentrations. Clouds developing in more polluted environments may be more efficient in separating charge and producing lightning (as evidenced by steeper slopes in the relationship between TLD and AVGHT30).

In accordance with previous observational studies, AVGHT30 was investigated here since it may provide a rough measure of updraft intensity. The assumption is that stronger updrafts are more capable of lofting cloud liquid and frozen hydrometeors. However, AVGHT30 is an ambiguous metric in this context since the same radar reflectivity can be realized for different hydrometeor populations [e.g., *Carey and Rutledge*, 2000]. We next examined VPRR for different stratifications of N40 in various thermodynamic environments to verify if the observed increases in lightning and AVGHT30 with respect to aerosols are associated with a more developed reflectivity column (Figure 11).

To investigate the possibility of simultaneous dependence on environmental thermodynamics, we stratified the data by NCAPE above the global median in addition to examining the full range of NCAPEs for both shallower and deeper WCD. Motivation for this part of the analysis came in part as a result of several aspects of the 30 dBZ echo top climatologies discussed in section 3; MAXHT30 did not change appreciably between continents and oceans (especially true for the global population of LPCFs). By the above method, we would be able to visualize potential differences in the response of vertical precipitation structure (i.e., the reflectivity column) in deep convective features at various levels of N40 in different thermodynamic environments.

For the global population of CFs (with and without lightning), a clear, systematic increase in reflectivity at a given altitude is shown as N40 increases from pristine levels (N40 $<100\,cm^{-3}$) to polluted levels (N40 $>500\,cm^{-3}$) for shallower and deeper WCD in all NCAPE environments. In agreement with the analysis in sections 3.2 and 3.4, the largest changes in VPRR at a given height with respect to N40 occur for shallower WCD (Figures 11a and 11c) compared to deeper WCD (Figures 11b and 11d). As shown in each inset, the difference in reflectivity between polluted and pristine profiles is maximized in the mixed phase region (greater for polluted features), and these differences are shown to vary slightly as a function of NCAPE. For all NCAPEs (Figures 11c and 11d), the difference between polluted and pristine environments ranges from 5.2 to 5.6 dB in the mixed phase. The observed mean VPRR for high NCAPE (VPRR with NCAPE above the global median value; NCAPE = $0.07\,J\,kg^{-1}\,m^{-1}$) illustrates that the magnitude of the difference in reflectivity within the mixed phase between polluted and pristine clouds is still appreciable (5.0–5.4 dB; Figures 11a and 11b).

The mean VPRR for various aerosol concentrations in different thermodynamic environments therefore shows that higher aerosol concentrations are associated with larger values of reflectivity at a given height

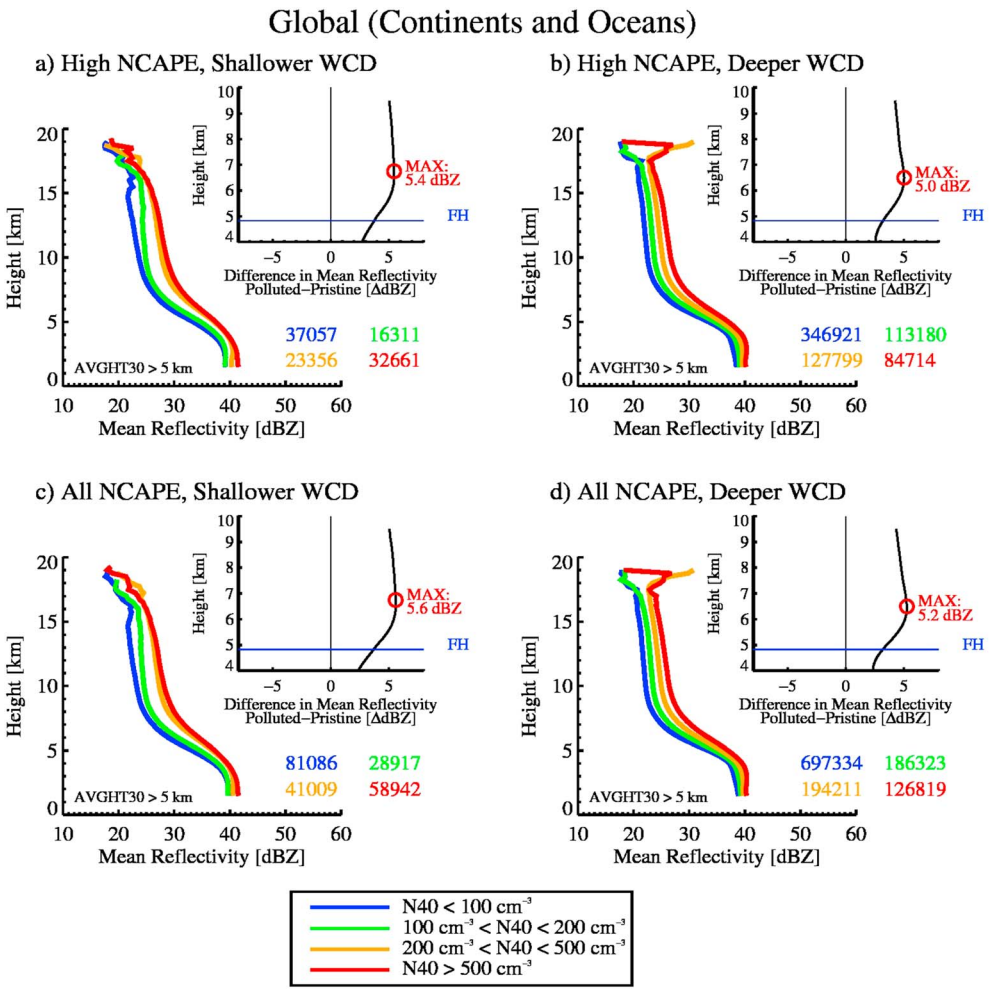

Figure 11. Mean vertical profiles of radar reflectivity (VPRR) for CFs across the global TRMM domain (continents and oceans) for various levels of N40 for (a) shallower WCD and (b) deeper WCD for NCAPE above the global median value (0.07 J kg^{-1} m^{-1}) and (c) shallower WCD and (d) deeper WCD for all NCAPEs. Colored values in the lower right of the main plots indicate the number of observations within each aerosol stratum. The differences between the most polluted and pristine VPRR are plotted for altitudes between 4 and 10 km in each inset. The altitude and magnitude of the maximum difference are provided by red open circles and adjacent text. The thin solid blue line in each inset indicates the global average height of the 0°C isotherm (4823 m). CFs with AVGHT30 >5 km were analyzed.

in the mixed phase. The behaviors of the mean VPRR, specifically in the mixed phase region, for different aerosol concentrations are consistent with previous hypotheses regarding aerosol indirect effects on deep convective clouds (e.g., R08) that greater latent heat release via transport of supercooled liquid water and subsequent riming/deposition processes lead to invigorated updrafts capable of lofting graupel. Additionally, we looked at the median TLD for each of the aerosol stratifications in the VPRR analysis; the median TLD increased monotonically between the pristine and polluted N40 stratifications consistent with the idea that greater flash rates/densities are associated with more vertically developed reflectivity. The results of the VPRR analysis also suggest that the influence of N40 on vertical precipitation structure decreases as NCAPE increases. A discussion of the foregoing results follows in the next section.

4. Discussion

We now summarize the behavior of deep convective features, associated lightning activity, and their mean VPRR signatures in differing background aerosol and thermodynamic environments (NCAPE and WCD). Our results suggest that *the highest TLD/AVGHT30 is found for deep convective features that develop in*

polluted environments where WCD is shallower and NCAPE is above the median value (Figures 3–6). Conditional sensitivities of convective intensity proxies (e.g., TLD and AVGHT30) illustrated that for a fixed WCD, increasing NCAPE resulted in greater TLD/higher AVGHT30 when N40 was above the median value (N40 $>$100–300 cm^{-3}) (Figures 7 and 8). Additionally, TLD and AVGHT30 were both nearly systematically larger for shallower WCD compared to deeper WCD (Figure 9). Note that the median value of WCD in our data was found to be very close to 4200 m; thus, "deeper" WCD probably represents the deepest limit of WCD globally. Thus, the results of this study favor a merged "simultaneous" hypothesis regarding the roles of thermodynamics and aerosols as they may influence the variability of deep convective clouds in the Tropics and subtropics.

Though a considerable amount of effort went into isolating the impacts of aerosols from background thermodynamics in our investigation of the variability of lightning and radar characteristics over continents and oceans, it is possible that other sources of potential variability exist within each respective environment (e.g., aerosol species, ice nuclei concentration, wind shear, and relative humidity in the middle troposphere). For example, the data from GEOS-Chem simulations used for this study made no distinction for ice nuclei, but ice nuclei sources, concentrations, and activity as a function of temperature are likely to differ between continents and oceans [e.g., *Burrows et al*., 2013]. In addition, environmental wind shear may impact the results of the current study through its connection to entrainment/mixing events in convective updrafts that could then influence CCN/ice nuclei concentrations and lead to changes in thermal buoyancy within cloudy parcels.

A combination of shallower WCD and more instability over continents implies that the warm cloud residence time for an ascending parcel could be sufficiently short to allow for efficient transport of cloud water to the mixed phase region to promote electrification and frequent lightning. While observations of very shallow WCD were absent from our tropical data set, we speculate that large TLD and high AVGHT30 may occur in these environments despite varying aerosol concentrations as the thermodynamics dictate the transport of cloud liquid water to the mixed phase region to allow for riming and charge separation. Additionally, for convective clouds with shallow WCD, the influence of aerosols on droplet growth processes may be limited as a result of the brief period of ascent through the cloud's warm phase. When WCD is $>$4000 m (e.g., for many oceanic regions in the Tropics), our findings (Figures 3–6) suggest that the activation of warm-rain microphysics and subsequent development of precipitation may still occur, even in the presence of high aerosol concentrations; this is substantiated by our results as the greatest TLD and highest AVGHT30 were found to occur in a relatively small region of the NCAPE-N40 parameter space (i.e., high NCAPE and high N40). Hence, it appears that the maximum sensitivity to aerosols in deep convective clouds should be found for environments with sufficient NCAPE for strong convective updrafts and shallower WCD (e.g., WCD $<$4000 m) in agreement with previous studies [e.g., *Wang*, 2005; *Fan et al*., 2007; *Mansell and Ziegler*, 2013].

TLD for a fixed AVGHT30 was found to vary considerably as a function of N40 especially for oceanic regions (Figure 10). In more polluted environments, the slope of the relationship between TLD and AVGHT30 is greater, and a given lightning density was associated with higher AVGHT30 in more pristine environments. The results suggest that lightning is sensitive to both changes in the internal vertical structure of precipitation and 30 dBZ echo top height. Meanwhile, we have shown that modest enhancements to reflectivity in the mixed phase region occur in progressively polluted boundary layer environments. While the correlation between lightning and radar reflectivity proxies for convective intensity is generally strong, their response to changes in thermodynamics and aerosol concentration may result from different processes.

For example, laboratory experiments suggest that at a constant temperature (i.e., altitude), the amount of charge separated per collision between ice particles increases with increasing supercooled liquid water content [*Takahashi*, 1978]. Thus, it is possible that increases in lightning with respect to increasing aerosol concentrations in a given thermodynamic environment result from enhanced transport of liquid water to the mixed phase region as warm-rain processes become less efficient for high aerosol concentrations, without invoking the convective invigoration hypothesis of R08. Meanwhile, increased reflectivities at a given height with increasing aerosol concentrations may again result from inefficient collision/coalescence and enhanced riming in the mixed phase, but larger particles have greater fall speeds. Therefore, a stronger updraft, possibly the result of enhanced latent heat release in the mixed phase when aerosol concentrations are high (e.g., R08), may be necessary to loft these particles to greater altitudes and contribute to larger reflectivity observed there.

In our examination of differences between the mean VPRR within deep CFs (i.e., CFs with AVGHT30 >5 km) for various stratifications of N40 (Figure 11), we noted distinct similarities in the mean vertical profiles but systematically larger reflectivity at a given height for progressively higher N40. *Szoke et al*. [1986] and *Zipser and Lutz* [1994] produced median VPRR for various samples of tropical oceanic, tropical continental, and midlatitude continental convective systems. The mean VPRR for CFs in pristine environments in our study depicted near constant reflectivity below the freezing level (near 40–45 dBZ) and rapid decreases in reflectivity above the freezing level—salient features of the VPRR shown by *Zipser and Lutz* [1994]. *Zipser and Lutz* [1994] showed differences of up to 10–15 dBZ above the freezing level between tropical oceanic and tropical continental convective systems.

We point out that the effect of aerosols is to "continentalize" the vertical precipitation structure by effectively enhancing the reflectivity above the freezing level. While differences in the mean VPRR with respect to aerosols are observed, they are still modest and vary quantitatively as a function of background thermodynamics. We interpret this finding as an indication that thermodynamics simultaneously influence the development of deep convection and are probably necessary to more accurately account for the full differences between tropical continental and tropical oceanic VPRRs and the observed lightning characteristics.

Lastly, it is possible that the response of TLD and AVGHT30 to thermodynamic characteristics of the environment and local concentrations of CCN varies seasonally and regionally. For example, Figure 9d illustrated that AVGHT30 was higher when WCD was deeper for low N40 and a considerable range of NCAPE for CFs over continents, in effect, countering the hypotheses concerning the role of WCD put forth by previous researchers [e.g., *Williams and Stanfill*, 2002; *Williams et al*., 2005; *Carey and Buffalo*, 2007]. Even though we exclude CFs and LPCFs with AVGHT30 <5 km in the current study to isolate the populations of deep CFs and LPCFs, we have chosen to incorporate CFs and LPCFs from the global-scale TRMM domain and continents and oceans, respectively. Therefore, it is possible that CFs and LPCFs from different background regimes (e.g., subtropical/midlatitude vs. deep tropical) in different stages of their respective life cycles are analyzed together. A pressing question then becomes whether the results found here are representative over continents and oceans everywhere or are there notable exceptions over finer time and space scales. Despite the limitation of the smaller sample sizes, a statistical decomposition of the relative influence of these independent variables on deep convection and lightning in specific seasons and regions of the Tropics and subtropics is underway.

5. Conclusion

In this study, we examined the variability of convective features observed by TRMM's precipitation radar and lightning imaging sensor in the Tropics between the years 2004 and 2011 in response to thermodynamics and boundary layer aerosol concentrations. The thermodynamic environment and aerosol concentration in the vicinity of deep convective clouds were characterized using reanalysis and a chemical transport model, GEOS-Chem. The advantage of our strategy arises from the continuity of reanalysis and model output as it allows for a large number of convective features in remote areas across the global Tropics and subtropics lacking in situ observations to be included in our data sample. Our objective was to use observations to validate a hypothesis put forth by *Rosenfeld et al*. [2008]—that aerosols modulate the release of conditional instability such that convective updrafts, radar reflectivity, and lightning are enhanced during the mature phase of convective cloud development.

In our global sample of deep convective features observed by the TRMM satellite, we found that TLD (AVGHT30) increased by more than 600% (2–3 km) as a function of both aerosol concentrations and thermodynamic instability simultaneously when WCD was held constant. The trends observed for the global populations of CFs and LPCFs were also found in the subsets of these populations over continents and oceans. Importantly, the changes in TLD and AVGHT30 with respect to NCAPE or N40 separately (holding other independent variables fixed) were comparable in many of the cases examined here. The partial sensitivities of TLD and AVGHT30 accounted for only a fraction of the total range of variability in the global populations of CFs and LPCFs when considering simultaneous changes with respect to both thermodynamics and aerosols. Meanwhile, TLD (AVGHT30) was shown to increase by up to 91% (1.25 km) between shallower and deeper WCD for a given combination of NCAPE and N40, with greater (higher) values shown in environments with shallower WCD. *Thus, total lightning density and the average height of*

30 dBZ echoes were maximized for high NCAPE, shallower WCD, and high N40 for the global population of deep convective CFs as well as over both continents and oceanic regions.

The relationship between TLD and AVGHT30 was shown to be strongly positive ($r = 0.95–0.98$) but variable as a function of background N40; the results suggest that clouds developing in more pristine environments must have 30 dBZ echoes reaching higher altitudes in order to produce similar lightning rates when compared to more polluted clouds. The mean reflectivity in the mixed phase region (~5–10 km altitude) of deep convective clouds was shown to be up to 5.6 dB higher in the most polluted environment relative to pristine environments, suggesting that increases in radar reflectivity within the mixed phase of a cloud occur when aerosol concentrations in the lower troposphere are higher. Finally, the analysis of VPRR illustrated that the differences in radar reflectivity at a given height in pristine and polluted clouds diminishes (the differences in reflectivity range from 5.0–5.4 dB) when NCAPE is above the global median value. We speculate that the impact of aerosols on the development of deep convection becomes less pronounced when NCAPE is high and WCD becomes progressively shallower.

This research represents the first effort to use a chemical transport model to more accurately attribute aerosol number concentrations to individual deep convective features in many thermodynamic environments in order to investigate their simultaneous influence on the variability of radar reflectivity and lightning between continents and oceanic regions on the global scale. Our findings provide observational evidence supporting a merged hypothesis for the impacts of thermodynamics and aerosols on deep convective clouds in the Tropics and subtropics. Meanwhile, we contribute new insight about the simultaneous influence of warm cloud depth.

Finally, the 35° inclination angle of the TRMM satellite meant that our results apply to deep convective clouds in the Tropics and subtropics only, i.e., clouds with intermediate to deeper WCD. With the advent of geostationary, continuous observations of total lightning in the future era of the GOES-R Global Lightning Mapper, it will be possible to conduct a study of this kind while covering nearly all possible combinations of NCAPE, N40, and WCD as they influence deep convective clouds.

Acknowledgments

The authors would like to acknowledge E. J. Zipser, B. Fuchs, E. J. Thompson, J. M. Peters, and B. O. Wolding, and two anonymous reviewers for their suggestions that led to improvements in our methodology. Salvatore Farina was instrumental in completing the GEOS-Chem TOMAS global chemical transport model simulations in a timely manner for this analysis. We acknowledge Paul Hein for his assistance with computing. The convective feature (CF) database is accessible online and may be downloaded via public http or anonymous ftp from the University of Utah server (ftp://trmm.chpc.utah.edu/pub/trmm/level_3/). Daily, 6-hourly data from the ERA-Interim Reanalysis were downloaded from the European Center for Medium Range Weather Forecasts online server (http://apps.ecmwf.int/datasets/data/interim_full_daily/). Information about the GEOS-Chem chemical transport model (www.geos-chem.org) with the online TOMAS aerosol microphysics module is available online (http://wiki.seas.harvard.edu/geos-chem/index.php/TOMAS_aerosol_microphysics). Data from the GEOS-Chem simulations analyzed in this study are available by special request (dstolz@atmos.colostate.edu). This research was supported by NASA PMM grant NNX13AG32G.

References

Adams, P. J., and J. H. Seinfeld (2002), Predicting global aerosol size distributions in general circulation models, *J. Geophys. Res.*, *107*(D19), 4370, doi:10.1029/2001JD001010.

Altaratz, O., I. Koren, Y. Yair, and C. Price (2010), Lightning response to smoke from Amazonian fires, *Geophys. Res. Let.*, *37*, L07801, doi:10.1029/2010GL042679.

Anderson, T. L., R. J. Charlson, D. M. Winker, J. A. Ogren, and K. Holmén (2003), Mesoscale variations of tropospheric aerosols, *J. Atmos. Sci.*, *60*, 119–136.

Andreae, M. O., and D. Rosenfeld (2008), Aerosol-cloud-precipitation interactions. Part 1: The nature and sources of cloud-active aerosol, *Earth Sci. Rev.*, *89*, 13–41.

Andreae, M. O., D. Rosenfeld, P. Artaxo, A. A. Costa, G. P. Frank, K. M. Longo, and M. A. F. Silva-Dias (2004), Smoking rain clouds over the Amazon, *Science*, *303*, 1337–1342, doi:10.1126/science.1092779.

Baker, B., M. B. Baker, E. R. Jayaratne, J. Latham, and C. P. R. Saunders (1987), The influence of diffusional growth rates on the charge transfer accompanying rebounding collisions between ice crystals and soft hailstones, *Q. J. R. Meteorol. Soc.*, *113*, 1193–1215.

Baker, M. B., and J. G. Dash (1994), Mechanism of charging between colliding ice particles in thunderstorms, *J. Geophys. Res.*, *99*(D5), 10,621–10,626, doi:10.1029/93JD01633.

Bell, T. L., D. Rosenfeld, K.-M. Kim, J.-M. Yoo, M.-I. Lee, and M. Hahnenberger (2008), Midweek increase in U.S. summer rain and storm heights suggests air pollution invigorates rainstorms, *J. Geophys. Res.*, *113*, D02209, doi:10.1029/2007JD008623.

Benedetti, A., et al. (2009), Aerosol analysis and forecast in the European Centre for Medium-Range Weather Forecasts Integrated Forecast System: 2. Data assimilation, *J. Geophys. Res.*, *114*, D13205, doi:10.1029/2008JD011115.

Blanchard, D. O. (1998), Notes and correspondence: Assessing the vertical distribution of convective available potential energy, *Weather Forecasting*, *13*, 870–877.

Boccippio, D. J., S. J. Goodman, and S. Heckman (2000), Regional differences in tropical lightning distributions, *J. Appl. Meteorol.*, *39*, 2231–2248.

Boccippio, D. J., W. A. Petersen, and D. J. Cecil (2005), The tropical convective spectrum. Part I: Archetypal vertical structures, *J. Clim.*, *18*, 2744–2769.

Burrows, S. M., C. Hoose, U. Pöschl, and M. G. Lawrence (2013), Ice nuclei in marine air: Biogenic particles or dust?, *Atmos. Chem. Phys.*, *13*, 245–267, doi:10.5194/acp-13-245-2013.

Carey, L. D., and K. M. Buffalo (2007), Environmental control of cloud-to-ground lightning polarity in severe storms, *Mon. Weather Rev.*, *135*, 1327–1353.

Carey, L. D., and S. A. Rutledge (2000), The relationship between precipitation and lightning in tropical island convection: A C-band polarimetric radar study, *Mon. Weather Rev.*, *128*, 2687–2710.

Cecil, D. J., S. J. Goodman, D. J. Boccippio, E. J. Zipser, and S. W. Nesbitt (2005), Three years of TRMM precipitation features. Part I: Radar, radiometric, and lightning characteristics, *Mon. Weather Rev.*, *133*, 543–566.

Christian, H. J., et al. (2003), Global frequency and distribution of lightning as observed from space by the Optical Transient Detector, *J. Geophys. Res.*, *108*(D1), 4005, doi:10.1029/2002JD002347.

Cifelli, R., W. A. Petersen, L. D. Carey, S. A. Rutledge, and M. A. F. da Silva Dias (2002), Radar observations of the kinematic, microphysical, and precipitation characteristics of two MCSs in TRMM LBA, *J. Geophys. Res.*, *107*(D20), 8077, doi:10.1029/2000JD000264.

D'Andrea, S. D., S. A. K. Häkkinen, D. M. Westervelt, C. Kuang, E. J. T. Levin, V. P. Kanawade, R. Leaitch, D. V. Spracklen, I. Riipinen, and J. R. Pierce (2013), Understanding global secondary organic aerosol amount and size-resolved condensational behavior, *Atmos. Chem. Phys.*, *13*, 11,519–11,534, doi:10.5194/acp-13-11519-2013.

Dee, D. P., et al. (2011), The ERA-Interim reanalysis: Configuration and performance of the data assimilation system, *Q. J. R. Meteorol. Soc.*, *137*, 533–597.
DeMott, C. A., and S. A. Rutledge (1998), The vertical structure of TOGA COARE convection. Part I: Radar echo distributions, *J. Atmos. Sci.*, *55*, 2730–2747.
Dusek, U., et al. (2006), Size matters more than chemistry for cloud-nucleating ability of aerosol particles, *Science*, *312*, 1375–1378, doi:10.1126/science.1125261.
Dye, J. E., W. P. Winn, J. J. Jones, and D. W. Breed (1989), The electrification of New Mexico thunderstorms. 1. Relationship between precipitation development and the onset of electrification, *J. Geophys. Res.*, *94*(D6), 8643–8656, doi:10.1029/JD094iD06p08643.
Fan, J., R. Zhang, G. Li, and W.-K. Tao (2007), Effects of aerosols and relative humidity on cumulus clouds, *J. Geophys. Res.*, *112*, D14204, doi:10.1029/2006JD008136.
Fan, J., L. R. Leung, D. Rosenfeld, Q. Chen, Z. Li, J. Zhang, and H. Yan (2013), Microphysical effects determine macrophysical response for aerosol impacts on deep convective clouds, *Proc. Natl. Acad. Sci. U.S.A.*, *110*(48), E4581–E4590, doi:10.1073/pnas.1316830110.
Graf, H. F. (2004), The complex interaction of aerosols and clouds, *Science*, *303*, 1309–1311, doi:10.1126/science.1094411.
Halverson, J. B., T. Rickenbach, B. Roy, H. Pierce, and E. R. Williams (2002), Environmental characteristics of convective systems during TRMM-LBA, *Mon. Weather Rev.*, *130*, 1493–1509.
Heiblum, R. H., I. Koren, and O. Altaratz (2012), New evidence of cloud invigoration from TRMM measurements of rain center of gravity, *Geophys. Res. Lett.*, *39*, L08803, doi:10.1029/2012GL051158.
Hudson, J. G., and S. Mishra (2007), Relationships between CCN and cloud microphysics variations in clean maritime air, *Geophys. Res. Lett.*, *34*, L16804, doi:10.1029/2007GL030044.
Iguchi, T., T. Kozu, R. Meneghini, J. Awaka, and K. Okamoto (2000), Rain-profiling algorithm for the TRMM precipitation radar, *J. Appl. Meteorol.*, *39*, 2038–2052.
Iribarne, J. V., and W. L. Godson (1981), *Atmospheric Thermodynamics*, 2nd ed., D. Reidel, Dordrecht, Netherlands.
Kelley, O. A., J. Stout, M. Summers, and E. J. Zipser (2010), Do the tallest convective cells over the tropical ocean have slow updrafts?, *Mon. Weather Rev.*, *138*, 1651–1672.
Khain, A. P., D. Rosenfeld, and A. Pokrovsky (2005), Aerosol impact on the dynamics and microphysics of deep convective clouds, *Q. J. R. Meteorol. Soc.*, *131*, 2639–2663, doi:10.1256/qj.04.62.
Khain, A. P., V. Phillips, N. Benmoshe, and A. Pokrovsky (2012), The role of small soluble aerosols in the microphysics of deep maritime clouds, *J. Atmos. Sci.*, *69*, 2787–2805.
Khain, A. P., T. Prabha, N. Benmoshe, G. Pandithurai, and M. Ovchinnikov (2013), The mechanism of first raindrops formation in deep convective clouds, *J. Geophys. Res. Atmos.*, *118*, 9123–9140, doi:10.1002/jgrd.50641.
Koren, I., G. Feingold, and L. A. Remer (2010), The invigoration of deep convective clouds over the Atlantic: Aerosol effect, meteorology or retrieval artifact?, *Atmos. Chem. Phys.*, *10*, 8855–8872, doi:10.5194/acp-10-8855-2010.
Koren, I., O. Altaratz, L. A. Remer, G. Feingold, J. Vanderlei Martins, and R. H. Heiblum (2012), Aerosol-induced intensification of rain from the tropics to the midlatitudes, *Nat. Geosci.*, *5*, 118–122, doi:10.1038/ngeo1364.
Lebo, Z. J., and H. Morrison (2014), Dynamical effects of aerosol perturbations on simulated idealized squall lines, *Mon. Weather Rev.*, *142*, 991–1009, doi:10.1175/MWR-D-13-00156.1.
Lee, S. S. (2012), Effect of aerosol on circulations and precipitation in deep convective clouds, *J. Atmos. Sci.*, *69*, 1957–1974, doi:10.1175/JAS-D-11-0111.1.
Lee, S. S., L. J. Donner, V. T. J. Phillips, and Y. Ming (2008), The dependence of aerosol effects on clouds and precipitation on cloud-system organization, shear and stability, *J. Geophys. Res.*, *113*, D16202, doi:10.1029/2007JD009224.
Li, Z., F. Niu, J. Fan, Y. Liu, D. Rosenfeld, and Y. Ding (2011), The long-term impacts of aerosols on the vertical development of clouds and precipitation, *Nat. Geosci.*, doi:10.1038/NGEO1313.
Liu, C., D. J. Cecil, E. J. Zipser, K. Kronfeld, and R. Robertson (2012), Relationships between lightning flash rates and radar reflectivity vertical structures in thunderstorms over the tropics and subtropics, *J. Geophys. Res.*, *117*, D06212, doi:10.1029/2011JD017123.
Lohmann, U., and J. Feichter (2005), Global indirect aerosol effects: A review, *Atmos. Chem. Phys.*, *5*, 715–737.
Lucas, C., E. J. Zipser, and M. A. LeMone (1994a), Convective available potential energy in the environment of oceanic and continental clouds: Corrections and comments, *J. Atmos. Sci.*, *51*, 3829–3830.
Lucas, C., E. J. Zipser, and M. A. LeMone (1994b), Vertical velocity in oceanic convection off tropical Australia, *J. Atmos. Sci.*, *51*, 3183–3193.
Mackerras, D., M. Darveniza, R. E. Orville, E. R. Williams, and S. J. Goodman (1998), Global lightning: Total, cloud, and ground flash estimates, *J. Geophys. Res.*, *103*(D16), 19,791–19,809, doi:10.1029/98JD01461.
Mansell, E. R., and C. L. Ziegler (2013), Aerosol effects on simulated storm electrification and precipitation in a two-moment bulk microphysics model, *J. Atmos. Sci.*, *70*, 2032–2050, doi:10.1175/JAS-D-12-0264.1.
May, P. T., V. N. Bringi, and M. Thurai (2011), Do we observe aerosol impacts on DSDs in strongly forced tropical thunderstorms?, *J. Atmos. Sci.*, *68*, 1902–1910.
Morcrette, J.-J., et al. (2009), Aerosol analysis and forecast in the European Centre for Medium-Range Weather Forecasts Integrated Forecast System: Forward modeling, *J. Geophys. Res.*, *114*, D06206, doi:10.1029/2008JD011235.
Morrison, H., and W. W. Grabowski (2013), Response of tropical deep convection to localized heating perturbations: Implications for aerosol-induced convective invigoration, *J. Atmos. Sci.*, *70*, 3533–3555, doi:10.1175/JAS-D-13-027.1.
Nesbitt, S. W., E. J. Zipser, and D. J. Cecil (2000), A census of precipitation features in the Tropics using TRMM: Radar, ice scattering, and lightning observations, *J. Clim.*, *13*, 4087–4106.
Niu, F., and Z. Li (2012), Systematic variations of cloud top temperature and precipitation rate with aerosols over the global tropics, *Atmos. Chem. Phys.*, doi:10.5194/acp-12-8491-2012.
Orville, R. E., and R. W. Henderson (1986), Global distribution of midnight lightning: September 1977 to August 1978, *Mon. Weather Rev.*, *114*, 2640–2653.
Petersen, W. A., and S. A. Rutledge (2001), Regional variability in tropical convection: Observations from TRMM, *J. Clim.*, *14*, 3566–3586.
Petersen, W. A., S. A. Rutledge, and R. E. Orville (1996), Cloud-to-ground lightning observations from TOGA COARE: Selected results and lightning location algorithms, *Mon. Weather Rev.*, *124*, 602–620.
Petersen, W. A., H. J. Christian, and S. A. Rutledge (2005), TRMM observations of the global relationship between ice water content and lightning, *Geophys. Res. Lett.*, *32*, L14819, doi:10.1029/2005GL023236.
Petersen, W. A., R. Fu, M. Chen, and R. Blakeslee (2006), Intraseasonal forcing of convection and lightning activity in the southern amazon as a function of cross-equatorial flow, *J. Clim.*, *19*, 3180–3196.

Pierce, J. R., and P. J. Adams (2009), Uncertainty in global CCN concentrations from uncertain aerosol nucleation and primary emission rates, *Atmos. Chem. Phys.*, *9*, 1339–1356, doi:10.5194/acp-9-1339-2009.
Pierce, J. R., M. J. Evans, C. E. Scott, S. D. D'Andrea, D. K. Farmer, E. Sweitlicki, and D. V. Spracklin (2013), Weak global sensitivity of cloud condensation nuclei and the aerosol indirect effect to Criegee + SO_2 chemistry, *Atmos. Chem. Phys.*, *13*, 3163–3176, doi:10.5194/acp-13-3163-2013.
Ramanathan, V. (2001), Aerosols, climate, and the hydrological cycle, *Science*, *294*, 2119–2124, doi:10.1126/science.1064034.
Reynolds, S. E., M. Brook, and M. F. Gourley (1957), Thunderstorm charge separation, *J. Meteorol.*, *14*, 426–436.
Rosenfeld, D. (1999), TRMM observed first direct evidence of smoke from forest fires inhibiting rainfall, *Geophys. Res. Lett.*, *26*(20), 3105–3108, doi:10.1029/1999GL006066.
Rosenfeld, D., and I. Lensky (1998), Satellite-based insights into precipitation formation processes in continental and maritime convective clouds, *Bull. Am. Meteorol. Soc.*, *79*(11), 2457–2476.
Rosenfeld, D., U. Lohmann, G. B. Raga, C. D. O'Dowd, M. Kulmala, S. Fuzzi, A. Reissell, and M. O. Andreae (2008), Flood or drought: How do aerosols affect precipitation?, *Science*, *321*, 1309–1313.
Rosenfeld, D., et al. (2014), Global observations of aerosol-cloud-precipitation climate interactions, *Rev. Geophys.*, *52*, 750–808, doi:10.1002/2013RG000441.
Rutledge, S. A., E. R. Williams, and T. D. Keenan (1992), The Down Under Doppler and Electricity Experiment (DUNDEE): Overview and preliminary results, *Bull. Am. Meteorol. Soc.*, *73*, 3–16.
Saunders, C. P. R. (1993), A review of thunderstorm electrification processes, *J. Appl. Meteorol.*, *32*, 642–655, doi:10.1175/15200450(1993)032<0642:AROTEP>2.0.CO;2.
Sherwood, S. C., V. T. J. Phillips, and J. S. Wettlaufer (2006), Small ice crystals and the climatology of lightning, *Geophys. Res. Lett.*, *33*, L05804, doi:10.1029/2005GL025242.
Stevens, B., and G. Feingold (2009), Untangling aerosol effects on clouds and precipitation in a buffered system, *Nature*, *461*(1), doi:10.1038/nature08281.
Stolz, D. C., S. Businger, and A. Terpstra (2014), Refining the relationship between lightning and convective rainfall over the ocean, *J. Geophys. Res. Atmos.*, *119*, 964–981, doi:10.1002/2012JD018819.
Storer, R. L., and S. C. van den Heever (2013), Microphysical processes evident in aerosol forcing of tropical deep convective clouds, *J. Atmos. Sci.*, *70*, 430–446.
Storer, R. L., S. C. van den Heever, and T. S. L'Ecuyer (2014), Observations of aerosol-induced convective invigoration in the tropical east Atlantic, *J. Geophys. Res. Atmos.*, *119*, 3963–3975, doi:10.1002/2013JD020272.
Szoke, E. J., E. J. Zipser, and D. P. Jorgensen (1986), A radar study of convective cells in mesoscale systems in GATE. Part I: Vertical profile statistics and comparison with hurricanes, *J. Atmos. Sci.*, *43*(2), 182–197.
Takahashi, T. (1978), Riming electrification as a charge generation mechanism in thunderstorms, *J. Atmos. Sci.*, *35*, 1536–1548.
Tao, W.-K., J.-P. Chen, Z. Li, C. Wang, and C. Zhang (2012), Impact of aerosols on convective clouds and precipitation, *Rev. Geophys.*, *50*, RG2001, doi:10.1029/2011RG000369.
van den Heever, S. C., and W. R. Cotton (2007), Urban aerosol impacts on downwind convective storms, *J. Appl. Meteorol. Climatol.*, *46*, 828–850.
van den Heever, S. C., G. L. Stephens, and N. B. Wood (2006), Aerosol indirect effects on tropical convection characteristics under conditions of radiative–convective equilibrium, *J. Atmos. Sci.*, *69*, 699–718.
van den Heever, S. C., G. L. Stephens, and N. B. Wood (2011), Aerosol indirect effects on tropical convection characteristics under conditions of radiative–convective equilibrium, *J. Atmos. Sci.*, *68*, 699–718.
van der Werf, G. R., J. T. Randerson, L. Giglio, G. J. Collatz, M. Mu, P. S. Kasibhatla, D. C. Morton, R. S. DeFries, Y. Jin, and T. T. Van Leeuwen (2010), Global fire emissions and the contribution of deforestation, savanna, forest, agricultural, and peat fires (1997–2009), *Atmos. Chem. Phys.*, *10*(23), 11,707–11,735, doi:10.5194/acp-10-11707-2010.
Varnai, T., and A. Marshak (2009), MODIS observations of enhanced clear sky reflectance near clouds, *Geophys. Res. Lett.*, *36*, L06807, doi:10.1029/2008GL037089.
Várnai, T., A. Marshak, and W. Yang (2013), Multi-satellite aerosol observations in the vicinity of clouds, *Atmos. Chem. Phys.*, *13*, 3899–3908, doi:10.5194/acp-13-3899-2013.
Venevsky, S. (2014), Importance of aerosols for annual lightning production at global scale, *Atmos. Chem. Phys. Discuss.*, *14*, 4303–4325.
Vesperini, M. (2002), ECMWF analyses of humidity: Comparisons to POLDER estimates over land, *Remote Sens. Environ.*, *82*, 469–480, doi:10.1016/S0034-4257(02)00070-6.
Wall, C., E. J. Zipser, and C. Liu (2014), An investigation of the aerosol indirect effect on convective intensity using satellite observations, *J. Atmos. Sci.*, *71*, 430–447.
Wang, C. (2005), A modeling study of the response of tropical deep convection to the increase of cloud condensation nuclei concentration: 1. Dynamics and microphysics, *J. Geophys. Res.*, *110*, D21211, doi:10.1029/2004JD005720.
Williams, E. R., and G. Sátori (2004), Lightning, thermodynamic and hydrological comparison of the two tropical continental chimneys, *J. Atmos. Sol. Terr. Phys.*, *66*, 1213–1231, doi:10.1016/j.jastp.2004.05.015.
Williams, E. R., and N. Renno (1993), An analysis of conditional instability of the tropical atmosphere, *Mon. Weather Rev.*, *121*, 21–36.
Williams, E. R., and S. Stanfill (2002), The physical origin of the land-ocean contrast in lightning activity, *C. R. Phys.*, *3*, 1277–1292.
Williams, E. R., et al. (1992), A radar and electrical study of tropical "hot towers", *J. Atmos. Sci.*, *49*, 1386–1395.
Williams, E. R., et al. (2002), Contrasting convective regimes over the Amazon: Implications for cloud electrification, *J. Geophys. Res.*, *107*(D20), (8082), doi:10.1029/2001JD000380.
Williams, E. R., T. V. Mushtak, D. Rosenfeld, S. Goodman, and D. Boccippio (2005), Thermodynamic conditions favorable to superlative thunderstorm updraft, mixed phase microphysics and lightning flash rate, *Atmos. Res.*, *76*, 288–306, doi:10.1016/j.atmosres.2004.11.009.
Yuan, T., L. A. Remer, K. E. Pickering, and H. Yu (2011), Observational evidence of aerosol enhancement of lightning activity and convective invigoration, *Geophys. Res. Lett.*, *38*, L04701, doi:10.1029/2010GL046052.
Yuan, T., L. A. Remer, H. Bian, J. R. Ziemke, R. Albrecht, K. E. Pickering, L. Oreopoulos, S. J. Goodman, H. Yu, and D. J. Allen (2012), Aerosol indirect effect on tropospheric ozone via lightning, *J. Geophys. Res.*, *117*, D18213, doi:10.1029/2012JD017723.
Zipser, E. J. (1994), Deep cumulonimbus cloud systems in the Tropics with and without lightning, *Mon. Weather Rev.*, *122*, 1837–1851.
Zipser, E. J., and K. R. Lutz (1994), The vertical profile of radar reflectivity of convective cells: A strong indicator of storm intensity and lightning probability?, *Mon. Weather Rev.*, *122*, 1751–1759.
Zipser, E. J., D. Cecil, C. Liu, S. Nesbitt, and D. Yorty (2006), Where are the most intense thunderstorms on Earth?, *Bull. Am. Meteorol. Soc.*, *87*, 1057–1071.